The Euphrates-Tigris-Karun river system: provenance, recycling and dispersal of quartz-poor foreland-basin sediments in arid climate

Eduardo Garzanti[1], Ali Ismail Al-Juboury[2], Yousef Zoleikhaei[3], Pieter Vermeesch[4], Jaafar Jotheri[5,6], Dicle Bal Akkoca[7], Ahmed Kadhim Obaid[5], Mark Allen[5], Sergio Andó[1], Mara Limonta[1], Marta Padoan[1], Alberto Resentini[1], Martin Rittner[4], Giovanni Vezzoli[1]

[1] Laboratory for Provenance Studies, Department of Earth and Environmental Sciences, University of Milano-Bicocca, 210126 Milano, Italy, eduardo.garzanti@unimib.it, sergio.ando@unimib.it, m.limonta1@campus.unimib.it, marta.padoan@unimib.it, alberto.resentini@unimib.it, giovanni.vezzoli@unimib.it

[2] Geology Department, Mosul University, Mosul, Iraq, alialjubory@yahoo.com

[3] School of Geology, University of Tehran, Tehran, yousef.zoleikhaei@yahoo.com

[4] London Geochronology Centre, Department of Earth Sciences, University College London, WC1E 6BT, UK, p.vermeesch@ucl.ac.uk, m.rittner@ucl.ac.uk

[5] Department of Earth Sciences, Durham University, Durham, DH1 3LE, UK, j.h.a.jotheri@durham.ac.uk, a.k.obaid@durham.ac.uk, m.b.allen@durham.ac.uk,

[6] Department of Archaeology, Al Qadisiyah University, Diwaniya, Iraq

[7] Department of Geological Engineering, Firat University, Elaziğ, Turkey, dbal@firat.edu.tr

Key words: Sedimentary petrology; Heavy minerals; U-Pb zircon geochronology; Anatolia-Zagros orogen; Undissected collision orogen provenance; Long-distance sediment transport.

ABSTRACT

We present a detailed sediment-provenance study on the modern Euphrates-Tigris-Karun fluvial system and Mesopotamian foreland basin, one of the cradles of humanity. Our rich petrographic and heavy-mineral dataset, integrated by sand geochemistry and U-Pb age spectra of detrital zircons, highlights the several peculiarities of this large source-to-sink sediment-routing system and widens the spectrum of compositions generally assumed as paradigmatic for orogenic settings. Comparison of classical static versus upgraded dynamic petrologic models enhance the power of provenance analysis, and allow us to derive a more refined conceptual model of reference and to verify the limitations of the approach.

Sand derived from the Anatolia-Zagros orogen contains abundant lithic grains eroded from carbonates, cherts, mudrocks, arc volcanics, obducted ophiolites and ophiolitic mélanges representing the exposed shallow structural level of the orogen, with relative scarcity of quartz, K-feldspar and mica. This quartz-poor petrographic signature, characterizing the undissected composite tectonic domain of the entire Anatolia-Iranian plateau, is markedly distinct from that of sand shed by more elevated and faster-eroding collision orogens such as the Himalaya. Arid climate in the region allows preservation of chemically unstable grains including carbonate rock fragments and locally even gypsum, and reduces transport capacity of fluvial systems, which dump most of their load in Mesopotamian marshlands upstream of the Arabian/Persian Gulf allochemical carbonate factory. Quartz-poor sediment from the Anatolia-Zagros orogen mixes with quartz-rich recycled sands from Arabia along the western side of the foreland basin, and is traced all along the Gulf shores as far as the Rub' al-Khali sand sea up to 4000 km from Euphrates headwaters.

A river watering the garden flowed from Eden; from there it was separated into four headwaters. The name of the first is the Pishon; it winds through the entire land of Havilah, where there is gold. The name of the second river is the Gihon; it winds through the entire land of Cush. The name of the third river is the Tigris; it runs along the east side of Ashur. And the fourth river is the Euphrates. Genesis 2:10-14

"Their reward from their Lord will be the gardens of Eden, wherein streams flow and wherein they will live forever. God will be pleased with them and they will be pleased with Him." Al-Quran 98:8

1. Introduction

Mesopotamia is the cradle of civilization. Bringing water and fertile sediments to an otherwise desert region, the Euphrates and Tigris Rivers allowed humans to settle, develop agricultural practices 10,000 years ago, learn how to domesticate animals, and produce the first book recorded in history, the Epic of Gilgamesh. Mesopotamia, a garden of Eden wounded by decades of war and unending atrocities committed in the name of God, is geologically speaking part of a subsiding foreland basin including the Arabian/Persian Gulf (Evans, 2011). The transition between the fluvial floodplain and the distal marine basin is - or was before the ecosystem collapsed under the impact of extensive drainage works and construction of large dams in Turkish headwaters (Partow, 2001) - the vast marshland well described by the British explorer Wilfred Thesiger in his book *Marsh Arabs*. Other streams join the trunk-river system, called here the Shatt al-Arab. These are the Karun, identified traditionally with the Gihon of the Genesis and draining the Zagros fold-thust belt in Iran, and Wadi Rimah/al Batin, held by some to be the Pishon of the Genesis, draining in ancient more humid times presently desert Arabia (Fig. 1).

Sediments of the Mesopotamian foreland basin are derived almost entirely from erosion of the Anatolia-Zagros composite orogen, grown during collision between Arabia and Eurasia preceded by ophiolite obduction in the Late Cretaceous (Alavi, 2004; Okay, 2008). The mountain belt runs along the southern front of the Anatolia-Iranian plateau, connecting the Alps and the Himalayas as part of the garland of ranges issued from Paleogene closure of the Neotethys Ocean (Dercourt et al., 2000). From the Taurus in the south to the Caucasus in the north, the region of distributed tectonic deformation is $\leq$ 1000 km in width and has elevations over 1500 m a.s.l. punctuated by volcanic peaks reaching above 5000 m a.s.l. (Yilmaz et al, 1998; Allen et al., 2013). Exposed in this wide tectonic domain are sedimentary strata, volcanic rocks and ophiolitic mélanges, with virtual absence of paleometamorphic crystalline basements and scarcity of high-pressure neometamorphic rocks (Şengör et al., 2003). Because sediments reflect the lithology of source terranes, those shed by the Anatolia-Zagros collision orogen are expected to be distinct compositionally from those generated in the Alps or the Himalayas, and characterized by abundant lithic grains from sedimentary and

volcanic rocks of the widely exposed supracrustal level. Characteristic of the Mesopotamian and Gulf regions is the arid climate, resulting in negligible chemical weathering and almost complete preservation of unstable detrital components. Because of the consequently limited erosion rates and fluvial-transport capacity, the Gulf represents today a rare case of partially underfilled marine foreland basin associated with a large collision orogen. Eolian sediment transport plays a major role in such an arid region. In the Pleistocene, during periods of low global sea-level, sand was deflated by reinforced northerly winds along the exposed floors of the Gulf and blown south and southwest up the Rub' al-Khali (Teller et al., 2000; Garzanti et al, 2003, 2013a).

This study investigates processes of erosion, transport and deposition at the subcontinental scale by using petrographic, mineralogical and geochronological signatures as tracers of long-distance multistep sediment dispersal. Besides the relevant archeological implications (Lees and Falcon, 1952; Morozova, 2005; Wilkinson et al., 2015), monitoring the compositional variability of modern sediments in big-river systems such as the Euphrates-Tigris-Karun drainage basin, over 10^6 km^2 wide and ranking about twentieth on Earth, provides us with a key to understand the information stored in sedimentary archives, and to reconstruct the evolution of the Earth's surface from the recent to the less recent past. Previous mineralogical studies on recent Mesopotamian sediments include Philip (1968), Berry et al. (1970), Ali (1976), Al-Juboury and Al-Miamary (2009) and Awadh et al. (2011).

2. The Anatolia-Zagros orogen

The Anatolia-Iranian plateau is a geological collage of microcontinents separated by ophiolitic sutures and eventually welded during collision between Arabia and Eurasia in the Paleogene (Robertson et al., 2013a). Late Cretaceous obduction is documented by both northern and southern ophiolitic belts of eastern Anatolia, which wrap around the Tauride microcontinent (Fig. 2). The northern (İzmir-Ankara-Erzincan) suture bends northeastward to continue in the Sevan-Akera suture of the Lesser Caucasus (Cavazza et al., 2015), whereas the southeast Anatolia orogen and the southern (Bitlis) suture bends southeastwards to continue in the Zagros Mountains across Iraqi Kurdistan (Fig. 3) and the northern coast of the Gulf (Fig. 4).

The Zagros orogen includes, from northeast to southwest (Agard et al., 2005): 1) subduction-related batholiths and volcanic rocks of the Urumieh-Dokhtar magmatic arc, representing the active southwestern margin of the Iranian microcontinent. The oldest plutonic rocks are Jurassic, with peak magmatic activity in the Eocene; the youngest volcanic products are Quaternary; 2) very-low-grade metasedimentary and metavolcanic rocks of the Sanandaj–Sirjan zone, including granitoid batholiths in the north and representing either an independent microcontinent detached from

Gondwana or part of the northern active margin of Neotethys (Alavi, 1994; Ghasemi and Talbot, 2006; Arfania and Shahriari, 2009); 3) a Late Cretaceous imbricate belt, including obducted ophiolites, limestones, radiolarites, turbidites and volcanic/metavolcanic rocks documenting the suture zone; 4) a Cenozoic fold-thrust belt, pierced by salt diapirs mostly rooted in Neoproterozoic-Cambrian evaporites, including a ≤ 13 km-thick sedimentary succession originally deposited during most of the Phanerozoic on the subsiding outer continental margin of Arabia (Sepehr and Cosgrove, 2004; Alavi, 2004); 5) the frontal foothills, including Neogene terrigenous sediments derived from the rising orogen (Al-Juboury et al., 2009a).

2.1. North Anatolia ophiolites and the Taurides

The Karasu headwater branch of the Euphrates flows along the Erzincan suture for ~200 km and next joins with the Murat River and several other tributaries draining the Tauride platform (Fig. 2). Exposed in the Erzincan region are the Upper Cretaceous Refahiye Ophiolite, consisting of serpentinized harzburgite with subordinate diabase and minor gabbro and plagiogranite, the associated mélange containing blocks of basalt, radiolarite and limestone, greenschist-facies arc volcanics, and turbidites. This rock assemblage is overlain in angular unconformity by upper Paleocene-Eocene shallow-marine carbonates and siliciclastics (Rice et al., 2009; Sarifakioğlu et al., 2009).

The Tauride platform includes Permo-Mesozoic carbonates overlain by ophiolitic mélange (Gürün and Munzur units) and a low-grade basement largely consisting of upper Paleozoic/lower Mesozoic metacarbonates (Malatya-Keban unit), cut by Upper Cretaceous granites and overlain by associated basaltic and andesitic lavas (Elazığ-Baskil arc complex; Robertson et al., 2007, 2013b). The overlying Cenozoic strata document major marine transgressions in the Eocene and early Miocene with widespread deposition of carbonates and siliciclastics. Throughout the late Neogene, eastern Anatolia was blanketed by shield and fissure eruptions of transitional tholeiitic-alkaline basalt, interfingering with fluvial and lacustrine deposits and extending to the Arabian foreland in the south (Pearce at al., 1990; Yilmaz et al., 1998).

2.2. The southeast Anatolia belt

The Tigris River is sourced in the southeast Anatolia belt and drains the Arabian platform south of it (Fig. 2). The metamorphic backbone of the range is the ~500 km-long and ~30 km-wide Bitlis-Pütürge massif, emplaced tectonically onto a polyphase ophiolitic mélange and volcano-sedimentary succession, separated in turn by a narrow belt of imbricated thrust slices from underlying Arabian continental-margin strata (Yilmaz, 1993). The massif, drained by the Batman

tributary of the Tigris, includes gneiss, micaschist and amphibolite of the Pan-African basement together with schist, metacarbonate and metavolcanics of its Paleozoic to lower Mesozoic cover (Ustaömer et al., 2012). Eclogites and blueschists formed during ophiolite obduction in the Late Cretaceous (Oberhänsli et al., 2010).

North of the metamorphic massif, three relatively undeformed to strongly deformed and partly metamorphosed Upper Cretaceous ophiolitic sequences are exposed west (İspendere), between (Kömürhan), and east (Guleman) of the Euphrates and Tigris courses (Robertson et al., 2007). South and east of the massif, dismembered ophiolites and island-arc assemblages include serpentinite, gabbro, basalt, radiolarite, limestone and clastic rocks of the Yüksekova mélange, as well as Eocene volcano-sedimentary successions deposited during final closure of Neotethys and equivalent to the Walash and Naopurdan Groups of Iraq (Yilmaz et al., 1993). These include the Maden Group, overlying the Bitlis-Pütürge massif and exposed in the Tigris headwaters, and the Helete volcanic rocks exposed across the drainage divide between the Euphrates and Cehyan rivers and possibly traced as far as the Kyrenia Range in north Cyprus (Yiğitbaş and Yilmaz, 1996). The largely marine Cambrian to Miocene succession of the Arabian foreland is best exposed in southeasternmost Turkey drained by the Greater Zab (Elmas and Yilmaz, 2003).

2.3. The Sanandaj-Sirjan zone

The Lesser Zab and Diyala tributaries of the Tigris, the Karkheh River, and the Dez tributary of the Karun all have their headwaters in the Sanandaj-Sirjan zone of Iran (Fig. 4). The volcano-sedimentary succession exposed in this 150-250 km-wide, NW/SE-elongated tectonic domain has experienced up to low-grade metamorphism. It includes Permo-Triassic metalavas, marbles and metasandstones, overlain by the 2-3 km-thick Hamedan phyllites, followed by Middle-Upper Jurassic clastics and limestones, and capped unconformably by Orbitolina limestones (Stocklin, 1968; Alavi, 1994). The domain includes Songor metavolcanics and chlorite-epidote schist; granodiorite to granite with minor tonalite and gabbro are common in the northern part (Agard et al., 2005).

The Shalair unit, which is part of the same domain and represents the structurally highest thrust-sheet in Iraq (Fig. 3), includes Paleozoic metamorphic rocks intruded locally by Upper Carboniferous granites, ≤ 500 m-thick imbricates of Upper Triassic carbonates, a thick volcano-sedimentary succession with phyllites and calcschists capped unconformably by Orbitolina limestones, and ~2 km-thick Upper Cretaceous andesites, dacites and rhyolites with superposed prehnite-pumpellyite to greenschist-facies metamorphism.

2.4. The Zagros suture

Geological descriptions of the suture zone, drained by Greater Zab and Lesser Zab tributaries in Iraq (Fig. 3) and by Diyala and Karkheh headwaters in Iran (Fig. 4), are taken mostly from Jassim and Goff (2006) and Agard et al. (2005). In Iraq, the Qulqula unit includes deformed radiolarites, carbonate turbidites and volcanic rocks of mostly Early Cretaceous age, and an upper thrust sheet of ~800 m-thick Triassic platform carbonates (Avroman Formation, partly equivalent to the Bisotun Formation in Iran). Permian limestones and thick conglomerates with limestone and chert clasts occur. Deposited originally onto the distal continental margin of Arabia as the Hawasina nappes of northern Oman, these strata were thrust onto the Arabian platform during Late Cretaceous obduction. The small Upper Cretaceous ophiolite complexes exposed in the area (Fig. 3) consist of sheared slivers or larger bodies of serpentinitized harzburgites or lherzolites, and incomplete crustal sequences including cumulates, gabbro, diorite, plagiogranite, and basaltic lava flows affected by low-grade metamorphism (e.g., Mawat Ophiolite; Aziz et al., 2011). These units are overlain unconformably by rudist-bearing Maastrichtian limestones and ~1 km-thick Paleogene red beds with intercalated Nummulitid limestones and conglomerates with boulders of chert and volcanic rocks.

The ≤ 4 km-thick Paleocene-Eocene arc volcanics and forearc turbidites of the Walash and Naopurdan Groups (Ali et al., 2013) are overthrust by a volcano-sedimentary sequence displaying greenschist to lower-amphibolite-facies metamorphism (Qandil series). Basalts, boninites and tuffs commonly show uralitization and extensive growth of amphibole, epidote or prehnite, and may be transformed into strongly foliated actinolite or chlorite schists. Blueschists occur locally. High-grade contact metamorphism was reached in the ≤ 2.5 km-wide aureole developed in sedimentary country rocks of the Eocene Bulfat gabbro.

In the adjacent Kermanshah region of Iran (Fig. 4), thrust-sheets stacked during Late Cretaceous obduction include ~500 m of strongly folded Jurassic-Cretaceous radiolarites, overthrust by ≤ 3 km-thick Upper Triassic to mid-Cretaceous Bisotun exotic shelfal limestones, and by ophiolite remnants including locally strongly serpentinized peridotites. Paleocene-Eocene arc-related volcanic rocks and turbidites are intruded by upper Eocene gabbros (Whitechurch et al., 2013).

2.5. The Zagros fold-thrust belt

The simply folded belt consists of largely competent carbonate rocks exposed in NW-SE trending parallel ridges drained by left-bank tributaries of the Tigris River in Iraq and by the Karun and Karkheh rivers in Iran. The base of the thick sedimentary succession, which rests on Precambrian metamorphic basement representing an extension of the Proterozoic Arabian shield, contains

uppermost Neoproterozoic/lowermost Cambrian dolostones and evaporites (e.g., Hormuz Salt) acting as a major detachment zone that controls the style of tectonic deformation (Bahroudi and Koyi, 2003). The overlying Paleozoic succession consists of shelfal clastic and carbonate rocks. In northernmost Iraq, ~4 km-thick Paleozoic strata are exposed in the Ora thrust zone drained by the Khabour River (Fig. 3), including Ordovician quartzose sandstones and mudrocks with *Cruziana* trace fossils, Devonian red beds with a volcanic interval, and Carboniferous sandstones, shales and minor limestones (Al-Juboury and Al-Hadidy, 2009). Upper Permian limestones and intercalated evaporites equivalent to the Khuff carbonates of Arabia document regional transgression following initial opening of Neotethys in the Early Permian (Angiolini et al., 2003). Triassic and Jurassic strata include variegated mudrocks intercalated with carbonates and evaporites, overlain by bituminous carbonates with sporadic chert nodules and black shales. The Cretaceous succession includes carbonate-ramp deposits, overlain by ~2 km-thick turbiditic sandstones and conglomerates with clasts of Mesozoic carbonate, radiolarian chert and green igneous and metamorphic rocks, interpreted to have been derived from, and deposited in front of advancing ophiolitic allochthons in the Campanian-Maastrichtian. Paleocene-Eocene strata include marls, sandstones and mudrocks with sporadic channelized conglomerate. The Neogene succession, gently folded and exposed in the foothills, consists of fluvio-deltaic red sandstones and mudrocks (Fat'ha or Lower Fars Formation; Al-Juboury and McCann, 2008) and ~3 km-thick, coarse-grained fluvio-deltaic sediments (Injana or Upper Fars and Bakhtiari formations; Al-Juboury, 2009).

The Neotethyan passive-margin succession in Iran includes ≥ 2 km-thick Permo-Triassic carbonates and evaporites unconformably overlain by lowest Jurassic siliciclastics passing upward to shallow-water limestones with *Lithiotis* (Szabo and Kheradpir, 1978). Deposition of carbonate-platform deposits, passing laterally to bituminous shales and evaporites, persisted until the Turonian. Late Cretaceous obduction was recorded by the disconformably overlying Santonian-Campanian marly limestones and shales, overlain by Maastrichtian sandstones and conglomerates with chert, serpentinite, volcanic and limestone clasts derived from the obducting ophiolites (Amiran Fm.), which are capped by the uppermost Cretaceous Tarbur carbonates. The 3-5 km-thick Cenozoic succession includes Paleogene dolostones, evaporites, sandstones and mudrocks, overlain by the upward-coarsening and southwest-prograding Neogene megasequence that includes carbonates (e.g., Asmari Fm.), siliciclastics and evaporites (Gachsaran Fm.), and finally "molassic" sandstones and fluvial conglomerates (Bakhtiari Fm.; Hessami et al., 2001).

3. The Euphrates-Tigris-Karun river system

The Euphrates-Tigris-Karun drainage basin exceeds 10^6 Km^2 and is about the twentieth largest on Earth (Fig. 1A). Fluvial management projects began over six millennia ago, until the second half of the last century when natural water and sediment fluxes were revolutionized by the construction of numerous major dams, the largest being the Atatürk Dam in southern Turkey with a capacity larger than the Euphrates annual flow.

3.1. The Euphrates River

The Euphrates (Firat/Furat) River, with a length of ~2800 km and a catchment of ~580,000 km^2, is the largest river of southwestern Asia. Its two upstream branches, the Karasu and Murat, rise in northeastern Anatolia at 3,290 and 3,520 m a.s.l., respectively. Mountainous headwaters have Mediterranean climate with hot dry summers and cold wet winters. Mean annual precipitation decreases progressively southward from ~1,000 mm in the mountains to ~300 mm near the Turkish/Syrian border, to 150 mm in Syria and only 75 mm in southern Iraq. Virtually all (88-98%) river water and sediments are generated in Anatolia. Peak discharge from rainfall and melting snow in April through May accounts for about half of annual runoff, which until the 1960s used to vary markedly at the Syrian border (17-43 km^3), partly as an effect of the North Atlantic climatic oscillation (Cullen and deMenocal, 2000). The natural river regime has changed drastically since construction of large dams and reservoirs between 1970 and 2000 for hydroelectric power, irrigation and flood control. These include the Keban Dam downstream of the Karasu/Murat confluence, the Karakaya Dam, the huge Atatürk Dam, the Birecik and Karkamiş Dams just upstream of the Syrian border, and the Tabqa (Buhayrat al-Assad) Dam in Syria. Little inflow is contributed by the arid plains of Syria, where the Khabur River represents the last significant tributary, and of Iraq, where widyan of the western desert may flow episodically during winter rains. After winding through a gorge 2-16 km-wide, the river eventually flows out on the Mesopotamian plain, where average annual discharge has dropped to 11 km^3, and peak discharge from 7500 m^3/s to 2500 m^3/s (Partow, 2001).

3.2. The Tigris River

The Tigris (Dicle/Dijlah) River, with a length of ~1850 km and a catchment of ~370,000 km^2, originates from Lake Hazar in the Taurus Mountains. The mild influence of the Mediterranean Sea decreases inland and to the south, causing a rapid shift to increasingly hot and dry conditions downstream. Precipitations are sparse in the Mesopotamian plain, with an annual average of 150-200 mm falling mainly in winter, whereas summers are hot and dry with temperatures up to 50°C.

The southern Anatolia headwater region contributes one-third to half of Tigris total annual water discharge (8-34 km^3 out of ~50 km^3), the rest being supplied by left-bank tributaries with perennial flow descending from the Zagros Mountains (Partow, 2001). These include the Khabour in northernmost Iraq, the Greater Zab sourced in southeasternmost Turkey, the Lesser Zab sourced in Iran, the Adhaim with its main Aqsu tributary, and the Diyala, sourced in Iran where it is called Sirwan and joining the Tigris just south of Baghdad. Water and sediment discharge has been reduced progressively through time by dam construction in Turkey (e.g., Dicle Dam, 1997), northern Iraq (Mosul Dam, 1986), and central Iraq (Samarra Dam, 1956; Kut Dam, 1939). Other dams with large reservoirs include the Dukan Dam on the Lesser Zab (1961) and the Darbandikhan Dam on the Sirwan/Diyala (1962).

3.3. The Mesopotamian floodplain

Because of arid climate, the life of plants, animals and humans in the Iraqi plains have always depended heavily on the availability of surface water. The Euphrates and Tigris river courses have seen continuous change in response to anthropic, autogenic and allogenic processes, causing damages to human settlements and irrigation systems due to flooding or desertification (Jotheri et al., 2016). Since the early Holocene, considerable efforts have been made by the Mesopotamian people to control and sustain the water for their requirements, and an extensive network of channels was formed over time throughout the region (Wilkinson et al., 2015). Downstream of the Hindiya Dam, the Euphrates divides into two channels joining again at Samawah. South of Nasiriyah the river flows through the Hawr el Hammar, where its sediment load is finally dumped before joining the Tigris south of Al-Qurnah. South of Baghdad, the slope of the Tigris River decreases progressively and meander curvature increases. At the Kut Dam, much of the river waters is diverted southward into the Shatt al-Gharraf, once the main river channel joining with the Euphrates at Nasiriyah (Fig. 1). More waters are lost through channels and marshes, and only 25% of the original discharge finally reaches the Euphrates confluence to form the Shatt al-Arab. Most of the sediment load is consequently deposited in the plains, and little is carried beyond Qalah Salih, ~60 km north of Al-Qurnah. Also the Karkheh River, which once joined the trunk river south of Al-Qurnah, breaks into several channels in the swampy area of southern Iraq, and along with the eastern branches of the Tigris is finally absorbed in the Hawizah Marshes straddling the Iraq/Iran border. Despite a potential annual load estimated at 105 million tons for the Euphrates and Tigris combined, the Shatt al-Arab upstream of the Karun confluence is thus virtually free of sediment (Partow, 2001).

3.4. Iranian rivers and the Shatt al-Arab

The highly sinuous, tectonically controlled courses of the Karkheh and Karun rivers drain the Zagros Mountains in Iran, where climate is hot and dry in summer and mild in winter, with annual precipitation decreasing sharply from 800 mm in the mountains to 150 mm in southern lowlands. The Karkheh River, the third longest in Iran, has a length of ~960 km, a catchment area of ~50,000 km^2, and a water discharge of ~5 km^3/a. The major Karkheh Dam, built in 2001 ~10 km upstream of the plains, never reached even close to full capacity and expected energy production because of low water levels. The Karun River, with a length of ~870 km and a catchment of ~70,000 km^2, has the highest discharge among all rivers in Iran (~20 km^3/a; Salarijazi et al., 2012). The mountain area comprises ~75% of the catchment, the rest being represented by the low-gradient plain where the trunk river is joined by the Dez tributary. Several dams were built in the basin from 1963 (Dez Dam) to 2010 (Karun-4 Dam), resulting in a reduction of sediment fluxes and increased levels of salinity in the Shatt al-Arab, thus damaging ecosystems and human activities (Afkhami, 2003). The river finally splits into two subparallel branches, one joining the Shatt al-Arab and the other flowing directly into the Gulf as the Bahmanshir River. In the Gulf, terrigenous sediments mix extensively with ooids and other allochems and are finally deposited in marine mudflats and sand bars (Aqrawi, 1994).

4. Methods

Field sampling in a region tormented by permanent war and conflict such as modern Iraq, Syria and southeastern Turkey is not easy. Between 2012 and 2016, very fine to medium-grained sands were collected wherever possible on active bars along the Euphrates River in Iraq and its major tributaries in Turkey (14 samples), along the Tigris River in Iraq and its major tributaries in Turkey, Iraq and Iran (44 samples), and along the Karkheh and Karun Rivers and their major tributaries in Iran as far as the Shatt al-Arab (17 samples). Sands derived from specific tectonic domains and carried by minor mountain rivers (first-order sampling scale of Ingersoll, 1990) were studied to identify the signatures of distinct source rocks, focusing in particular on the ophiolitic suture zone of Iraqi Kurdistan drained by the Qara Cholan River (Fig. 3). The complete set of 94 samples also includes 1 eolian dune and 16 Mesopotamia floodplain sediments in Iraq, 1 sample from Wadi al-Batin in Saudi Arabia, and 1 Gulf beach in Kuwait. Information on sample location is provided in Appendix Table A1 and Supplementary file *EuTiKa.kmz*.

4.1. Petrography and heavy minerals

A quartered fraction of each sample was impregnated with Araldite, cut into a standard thin section, stained with alizarine red to distinguish dolomite and calcite, and analysed by counting 400 points under the microscope (Gazzi-Dickinson method; Ingersoll et al., 1984; Zuffa, 1985). Sand classification is based on the main components quartz, feldspars and lithic fragments considered if exceeding 10%QFL (e.g., a sand is named quartzo-lithic if L > Q > 10%QFL > F; Garzanti, 2016). Metamorphic grains were classified by protolith composition and metamorphic rank. Average rank of rock fragments in each sample is expressed by the metamorphic indices MI and MI*. MI varies from 0 (detritus shed by sedimentary and volcanic cover rocks exclusively) to 500 (very-high-rank detritus exclusively shed by high-grade basement rocks). MI* considers only metamorphic rock fragments and thus varies from 100 (very-low-rank detritus shed by very low-grade metamorphic rocks) to 500 (Garzanti and Vezzoli, 2003). The Sc/S ratio (peridotite and lizardite-serpentinite grains with preserved cellular texture over total ultramafic grains including foliated antigorite-serpentineschist) allows distinction of detritus from relatively undeformed obducted peridotites versus strongly deformed subducted mantle rocks (Garzanti et al., 2002a). Median grain size was determined in thin section by ranking and visual comparison with sieved standards.

Although bulk-sample analyses represent the only correct option to estimate percentages of heavy minerals accurately, the presence of grains with great size differences in poorly sorted sands makes mounting and identification difficult. For such practical reasons a size window must be chosen, which should be wide enough to obtain a faithful characterization of the detrital assemblage (Garzanti et al., 2009). Heavy-mineral analyses were carried out on a 3.5 to 5 ϕ-wide size window (32-355 μm to 15-500 μm) obtained by dry sieving. Even with such a large window, the 10 ± 10% (fine tail) and 11 ± 17% (coarse tail) of the bulk sample were excluded from analysis. Heavy minerals were separated by centrifuging in sodium polytungstate (density ~2.90 g/cm^3), and recovered by partial freezing with liquid nitrogen. On grain mounts, ≥ 200 transparent heavy-mineral grains were either counted under the microscope by the area method or point-counted at suitable regular spacing to obtain real volume percentages (Galehouse, 1971). Heavy-mineral concentrations, calculated as the volume percentage of total (HMC) and transparent (tHMC) heavy minerals (Garzanti and Andó, 2007a), range from "very poor" (tHMC < 0.5) and "poor" (0.5 ≤ tHMC < 1) to "rich" (5 ≤ tHMC < 10), "very-rich" (10 ≤ tHMC < 20) and "extremely rich" (20 ≤ tHMC < 50). The ZTR index, expressing the "mineralogical stability" of the suite, is the sum of zircon, tourmaline and rutile over total transparent heavy minerals (Hubert, 1962). The "Hornblende Colour Index" HCI (Andó et al., 2014) varies from 0 in detritus from lowermost amphibolite-facies rocks yielding blue-green amphibole exclusively, to 100 in detritus from granulite-facies or

volcanic rocks yielding brown amphibole exclusively. Significant minerals are listed in order of abundance throughout the text. Key petrographic and mineralogical parameters are shown in Table 1. The complete petrographic and mineralogical datasets are provided in Appendix Tables A2 and A3.

4.2. Geochemistry and U-Pb zircon geochronology

Chemical analyses of 20 selected samples were carried out at ACME Laboratories (Vancouver) on a split aliquot of the 63-2000 μm fraction obtained by wet sieving. Major oxides and some minor elements were determined by ICP-ES and trace elements by ICP-MS, following a lithium metaborate/tetraborate fusion and nitric acid digestion. A separate split was digested in aqua regia and analysed for Mo, Ni, Cu, Ag, Au, Zn, Cd, Hg, Tl, Pb, As, Sb, Bi, Se, but the concentration of these elements may be underestimated because of only partial leaching of refractory minerals. For further information on adopted procedures, geostandards used and precision for various elements see http://acmelab.com (group 4A-4B and code LF200).

The U-Pb ages of detrital zircons identified by Qemscan electron microscopy on the heavy-mineral separates of 25 selected samples were determined at the London Geochronology Centre using an Agilent 7700 LA-ICP-MS system, employing a New Wave NWR193 Excimer Laser operated at 10 Hz with a 20 μm spot size and ~2.5 J/cm^2 fluence. Each analysis comprised 15 s of laser warm-up time during which blanks were measured, followed by 27 s of laser ablation and 18 s of washout delay. Signal selection and data interpolation were done using GLITTER© software (Griffin et al., 2008). The first 2 s of the laser ablation were discarded, and the remaining signal was normalised to the Plešovice zircon standard (Sláma et al. 2008). To avoid grain-to-grain bias and treat all the samples equally, the laser spot was always placed in the core of zircon grains; no CL-imaging was done. We used $^{206}Pb/^{238}U$ and $^{207}Pb/^{206}Pb$ ages for zircons younger and older than 1100 Ma, respectively. No common Pb correction was applied. Grains with > 10% age discordance were discarded, and thus only 9 samples yielded more than 50 usable ages; 1164 ages were used overall. Key geochemical parameters are shown in Table 2. The full geochemical and geochronological datasets are provided in Appendix Tables A4 and A5.

5. Detrital fingerprints

In this section we illustrate the petrographic and mineralogical composition of sand generated, transported and deposited in the vast catchment of the Euphrates, Tigris and Karun Rivers (Fig. 5). Their geochemical and geochronological signatures are described next.

5.1. Euphrates sands

The Euphrates River carries to central Iraq feldspatho-quartzo-lithic sand with intermediate to mafic volcanic, carbonate, serpentinite, chert, and minor metamorphic rock fragments (Fig. 5D). The rich epidote-clinopyroxene-amphibole suite includes hypersthene, garnet, apatite, oxy-hornblende, Cr-spinel and olivine.

In Turkish headwaters, sand of the Murat tributary is similarly feldspatho-quartzo-lithic, including common volcanic and metavolcanic, subordinate limestone and granitoid, and minor chert and serpentinite grains, as well as rich amphibole-clinopyroxene-epidote suites with some garnet (Fig. 6). Karasu sand upstream of Erzincan is instead feldspatho-lithic ultramaficlastic with subequal serpentineschist and cellular serpentinite, abundant volcanic/metavolcanic, carbonate and other sedimentary rock fragments; the rich clinopyroxene-dominated suite includes amphibole, epidote, minor Cr-spinel, garnet, enstatite and olivine. Volcanic detritus increases markedly downstream, and sand entering the Keban reservoir is feldspatho-lithic with lathwork and microlitic volcanic grains; dominant augitic clinopyroxene is associated with hypersthene and oxy-hornblende. Other Anatolian tributaries carry sand varying in composition from quartzo-feldspatho-lithic carbonaticlastic with abundant biotite and micaschist lithics (Munzur), to lithic with abundant carbonate, volcanic/metavolcanic and cellular serpentinite grains (Pülümur), to feldspato-quartzo-lithic volcaniclastic (Perisuyu) or lithic carbonaticlastic (Tohma). Moderately rich to rich heavy-mineral suites range from clinopyroxene-dominated (Munzur, Tohma) to amphibole-clinopyroxene-epidote (Pülümur, Perisuyu), and may contain common grossular or almandine garnet, hypersthene, Cr-spinel, enstatite, olivine or apatite, and locally glaucophane.

5.2. Tigris sands

The Tigris River carries to central Iraq feldspatho-quartzo-lithic sedimentaclastic sand including carbonate, shale/slate, chert, volcanic/metavolcanic and a few serpentinite rock fragments (Fig. 5E). The moderately rich to rich epidote-garnet-amphibole-clinopyroxene suite includes Cr-spinel.

In southeastern Anatolian headwaters, sand is quartzo-feldspatho-lithic volcaniclastic with limestone, shale/slate and serpentinite grains. The rich to very rich heavy-mineral assemblage mainly includes epidote, clinopyroxene and amphibole, with olivine, garnet, enstatite and minor andalusite. The major Batman tributary carries feldspatho-litho-quartzose metamorphiclastic sand including granitoid, metavolcanic and serpentinite rock fragments, and a moderately rich epidote-amphibole-garnet suite (Fig. 5A). Downstream of the Batman confluence, Tigris sand becomes

litho-feldspatho-quartzose metamorphiclastic with a moderately rich garnet-epidote-amphibole suite, quite similar to Batman sand.

In Iraq downstream of the Khabour confluence, sand is feldspatho-quartzo-lithic sedimentaclastic with a garnet-epidote-amphibole-clinopyroxene suite including Cr-spinel. Composition does not change much downstream of the Greater Zab confluence. Between the Lesser Zab and Adhaim confluences, river sand and adjacent eolian dunes are feldspatho-litho-quartzose with rounded quartz, lower heavy-mineral concentration, less amphibole, negligible pyroxene, and relatively more common epidote, garnet, zircon, tourmaline and rutile.

5.3. Sands of Tigris tributaries in Iraq

The Khabour River carries quartzo-lithic carbonaticlastic sand including mainly plagioclase feldspar and common microclitic volcanic, shale/siltstone, chert and minor low-rank metamorphic and serpentinite rock fragments. The poor heavy-mineral suite includes epidote, Cr-spinel, clinopyroxene, amphibole and minor titanite, garnet and apatite.

The Greater Zab carries lithic sedimentaclastic sand with common carbonate, intermediate to mafic volcanic, shale/slate, cellular serpentinite, and minor chert, metavolcanic and schist lithic fragments. The rich, clinopyroxene-dominated suite includes common amphibole and epidote, rare titanite, apatite, Cr-spinel, and locally glaucophane.

The Lesser Zab carries quartzo-lithic sedimentaclastic sand with limestone, shale/slate, chert, felsic to mafic volcanic, schist and serpentinite rock fragments (Fig. 5B). The moderately rich, epidote-amphibole-clinopyroxene suite includes garnet and minor andalusite, oxy-hornblende and Cr-spinel. Sands in Iranian headwaters range from quartzo-lithic to feldspatho-quartzo-lithic sedimentaclastic, with moderately poor amphibole-epidote to very rich amphibole-clinopyroxene-epidote suites with some garnet. In Iraq upstream of Lake Dukan, sand is quartzo-lithic sedimentaclastic as in the final tract, but with more metamorphic rock fragments, biotite and heavy minerals, and less chert and volcanic rock fragments; the moderately rich heavy-mineral suite is notably enriched in andalusite. Downstream of Lake Dukan, sand is depleted in heavy-minerals and enriched in chert, dolostone, volcanic and serpentinite rock fragments.

The Aqsu tributary of the Adhaim River and a minor tributary of the Lesser Zab with ephemeral seasonal flow draining entirely within Cenozoic strata of the Zagros foothills carry lithic to quartzo-lithic sedimentaclastic sands dominated by chert, limestone and shale/slate grains with subordinate volcanic/metavolcanic grains (Fig. 5C). Heavy-mineral suites are poor to moderately poor and epidote-dominated with some garnet, amphibole, clinopyroxene and Cr-spinel.

The Diyala River carries lithic sedimentaclastic sand dominated by chert, limestone and shale associated with volcanic/metavolcanic grains. The moderately poor, clinopyroxene-epidote-amphibole suite includes oxy-hornblende and garnet. In Iranian headwater branches, sand is quartzo-feldspatho-lithic sedimentaclastic with shale/slate, limestone, volcanic and metabasite grains, and includes either moderately rich epidote-dominated or rich clinopyroxene-amphibole-epidote-garnet suites. Downstream of the Zagros suture, Sirwan sand is notably enriched in limestone, chert and pyroxene grains, and includes oxy-hornblende, hypersthene, andalusite and olivine.

5.4. Mesopotamian foreland-basin sediments

Sand of the Mesopotamian floodplain between Baghdad and Al-Qurnah is predominantly feldspatho-quartzo-lithic sedimentaclastic with carbonate, lathwork to microlitic volcanic, serpentinite and a few metamorphic, shale and chert grains (Fig. 5G). The rich amphibole-clinopyroxene-epidote suite includes minor garnet, Cr-spinel, orthopyroxenes, prehnite, and locally pumpellyite and glaucophane. Detrital modes are intermediate between Euphrates and Tigris sands, with Euphrates contribution prevailing in the northwest and Tigris contribution in the southeast (Fig. 6). Extensive mixing and homogenization in the floodplain is the result of numerous avulsion episodes with lateral migration and repeated bifurcation of trunk-river channels during the Quaternary (Jotheri et al., 2016). Even the composition of modern Euphrates sand collected at Nasiriyah indicates mixing with sediments transported by right-bank distributaries of the Tigris (e.g., Shatt al-Gharraf) and/or reworked from the floodplain. Some floodplain sands collected west of the Euphrates in the Karbala region are litho-feldspatho-quartzose or even quartzose, with much poorer heavy-mineral suites enriched slightly in zircon, tourmaline and rutile, which indicates mixing with sand recycled from the Arabian foreland in the southwest (Fig. 5H).

The upper Miocene Injana Formation in northernmost Iraq consists of quartzo-feldspatho-lithic carbonaticlastic sandstone yielding magnetite, ilmenite, Cr-spinel, amphibole, pyroxene, epidote, garnet, zircon, tourmaline and rutile (Al-Juboury, 2009). Quartz steadily increases southward, reaching maximum in the Karbala area (fig. 8 in Al-Juboury, 2009). Heavy-mineral data from Pleistocene terraces and Neogene molassic wedges (Philip, 1968) document a consistent compositional pattern since the late Miocene at least, with notably unchanged epidote-amphibole-pyroxene suites in the Euphrates valley and epidote-dominated suites in the Adhaim catchment.

5.5. Karkheh and Karun sands

The Karkheh River carries lithic carbonaticlastic sand with chert and a few volcanic and serpentinite rock fragments. The poor epidote-clinopyroxene-amphibole suite includes Cr-spinel, garnet, andalusite, and minor tourmaline, apatite and oxy-hornblende. Detritus in the small Jamishan headwater tributary is far richer in plagioclase and volcanic rock fragments, and contains more very-low-rank metasedimentary and metavolcanic grains and far less chert; the rich clinopyroxene-epidote-amphibole suite includes olivine but little Cr-spinel. Sand collected at Jalogir downstream of the Kashkan confluence yielded abundant gypsum grains and a very poor transparent-heavy-mineral suite dominated by celestite.

The Karun River carries lithic carbonaticlastic sand with chert and other sedimentary grains (Fig. 5F). The poor/very poor epidote-clinopyroxene-amphibole suite includes Cr-spinel and garnet, and minor zircon, tourmaline, andalusite and oxy-hornblende. Sand of its Dez tributary is lithic cherticlastic-carbonaticlastic and includes abundant carbonate and rare volcanic lithics, relatively common pyroxene and amphibole, and some andalusite.

5.6. Shatt al-Arab, Wadi al-Batin and Gulf sands

Sand in the Shatt al-Arab estuary has the very same lithic carbonaticlastic signature as Karun sand (Fig. 5I), indicating negligible contribution from the Tigris and Euphrates. Since long before construction of large dams and irrigation canals, the two rivers have dumped their load upstream of their confluence in Iraqi marshlands (Berry et al., 1970; Baltzer and Purser, 1990; Aqrawi and Evans, 1994), which act as a very efficient sediment trap much as the Sudd Marshes along the White Nile in South Sudan (Garzanti et al., 2015).

Wadi al-Batin, which once represented the lower tract of Wadi Rimah connecting interior Arabia to the Gulf, contains sand dominated by mainly monocrystalline quartz grains commonly showing abraded overgrowths, with a few carbonate grains and feldspars. The very poor heavy-mineral suite includes amphibole, zircon, clinopyroxene, rutile, epidote, and minor tourmaline.

The terrigenous fraction of beach sand in Kuwait, mixed with abundant ooids and some bioclasts, is almost as quartzose as Wadi al-Batin sand but includes a little more plagioclase and K-feldspar, and some mafic volcanic, metavolcanic and metabasite rock fragments (Fig. 6). Instead, the extremely poor heavy-mineral suite closely resembles Shatt al-Arab sands, being rich in epidote associated with clinopyroxene, amphibole and garnet, and including enstatite, hypersthene, oxy-hornblende and Cr-spinel, with only a few zircon, tourmaline and rutile grains.

5.7. Geochemistry

Traditional geochemical approaches are scarcely applicable to Mesopotamian foreland-basin sediments, derived largely from sedimentary strata, volcanic fields and obducted ophiolites, because of their quartz-poor composition with abundant carbonate grains. Comparison with the upper continental crust standard (UCC; Taylor and McLennan, 1995) hardly makes sense. Classical indices such as the CIA (Nesbitt and Young, 1982) or the WIP (Parker, 1970) are of little use because the correction needed for CaO hosted in carbonates is huge and no correction method is robust (Garzanti and Resentini, 2016). The use of the CIA/WIP ratio as an indicator of recycling (Garzanti et al., 2014) is also prevented. The CIA uncorrected for CaO in carbonates is ≤ 30 for most samples, and reaches as low as 10 for Karkheh sand and ≤ 5 for Karun and Shatt al-Arab sands, reflecting abundance of carbonate grains. Scarcely meaningful are also α^{Al} values (Garzanti et al., 2013a), which are generally very low for elements hosted in carbonates (0.01-0.7 for Ca, 0.1-0.8 for Mg, 0.1-1.5 for Sr) and vary mostly between 1 and 2 for Na, K and Ba, depending on the mineralogy of source rocks rather than on weathering conditions. On the other hand, the widespread and commonly overwhelming presence of carbonate grains is a sufficient indicator that weathering is negligible, as expected given the arid climate through most of the catchment. Sand remains unweathered in the floodplain to a depth of at least some meters, as indicated by unchanged compositional parameters with burial depth. Worthy of note is that the scarcity in quartz does not translate automatically to low SiO_2, because chert-rich Aqsu and Diyala sands display SiO_2 concentrations close to 80% (Table 2). Distinguishing on purely geochemical ground these sands from quartz-rich sediments derived instead from the Arabian foreland would not be straightforward.

Relative to litho-feldspatho-quartzose metamorphiclastic Ganga-Brahmaputra sediments, derived dominantly from the Himalaya but partly also from the Indian foreland and taken here as a reference for foreland-basin sands (Garzanti et al., 2010), Mesopotamian sands show concentration of Ca and loss on ignition higher by factors of 4 (Euphrates), 5 (Tigris) or even 10-15 (Karun and Shatt al-Arab), and higher by factors of 2-3 for Mg and Sr. In Tigris, Euphrates, Karkheh and Karun sands, Cr is higher by an order of magnitude; Mo, Ni, Cu and As are also markedly higher. Notably higher in Euphrates and Tigris sands are Sc, V and Co as well. In Wadi al-Batin sand, instead, the overwhelming abundance of quartz recycled from quartzose siliciclastic cover of the Arabian foreland is reflected in dominant Si and marked depletion of all other elements.

5.8. Detrital-zircon geochronology

From the Euphrates sand collected at Nasiryiah, 147 concordant U-Pb zircon ages were obtained. They show minor clusters at 21 Ma (2% of total zircons), 70-77 Ma (6%), 93-98 Ma (2%) and 307-310 (2%), and a Paleozoic scatter (325-522; 7%). The dominant peak is between 530 and 662 Ma

(37%), followed by a cluster (752-848; 12%) and a scatter (865-1048 Ma; 14%) in the Neoproterozoic, by a 0.8 Ga-long gap, some ages around 1.85 Ga and 2.5 Ga (7% overall) with a maximum of 2701 Ma.

From three Tigris sands collected north, at, and south of Baghdad, 215 concordant U-Pb zircon ages were obtained. They show an Oligocene-Late Cretaceous peak (25-102 Ma; 16% of total zircons), minor mid-Jurassic and Late Triassic clusters (166-170 and 225-230 Ma; 3%), a Carboniferous peak (294-349 Ma; 11%), and a mid-Paleozoic scatter (358-493 Ma; 8%). The dominant peak is between 500 and 666 Ma (39%), followed by a Neoproterozoic scatter (680-958 Ma; 10%), minor clusters around 1.8 Ga and 2.4 Ga (4% overall) with a maximum of 3265 Ma.

From nine Karun and Shatt al-Arab sand samples, 789 concordant U-Pb zircon ages were obtained. They show ages from as young as 6-8 Ma (< 1%) to as old as 2665-3260 Ma (1%). Minor clusters occur at 30-68 Ma (3%) and 87-98 Ma (1%), a major peak at 141-192 Ma (12%), and clusters at 203-346 Ma (13%), 364-383 Ma (1%) and 393-469 Ma (5%). Older ages are mostly concentrated between 485 and 1090 Ma (44%), between 1685 and 1722 (1%), between 1787 and 1986 Ma (8%), and between 2407 and 2632 Ma (6%).

Karun and Shatt al-Arab sands, most readily distinguished by many Jurassic to Permian zircon ages virtually lacking in Euphrates sand and scarcely represented in Tigris sand, are characterized also by late Miocene, early Paleozoic, Mesoproterozoic to late Paleoproterozoic, and early Paleoproterozoic ages. Age spectra are sufficiently distinct from those shed from Arabian sources (Garzanti et al., 2013a) to conclude that only a few zircon grains may be recycled from sandstones intercalated in the carbonate-dominated succession accreted in the Zagros fold-thrust belt and originally derived from Arabia. Tigris sand is characterized by late Oligocene ages, Eocene ages, and Paleozoic clusters at ~320 and ~540; Euphrates sand by early Miocene ages, latest Cretaceous ages, and Neoproterozoic clusters at ~600, ~650 and ~840 (Fig. 7).

6. Provenance and recycling of quartz-poor orogenic sands

In contrast to the adjacent Alpine and Himalayan collision orogens where various neometamorphic and paleometamorphic rocks are exposed, the composite Anatolia-Zagros orogen drained by the Euphrates, Tigris and Karun rivers consists largely of sedimentary strata, volcanic to low-grade metavolcanic rocks and ophiolites. As a consequence of both arid climate and geological history, including Late Cretaceous obduction followed by collision in the Cenozoic, both first-cycle and recycled Mesopotamian foreland-basin sands are remarkably quartz-poor. They display high plagioclase/feldspar ratio and abundant carbonate grains associated with chert,

volcanic/metavolcanic and ultramafic rock fragments, pyroxenes and Cr-spinel. Such a signature characterizes detritus shed from broad undissected orogenic domains such as the Anatolia-Iranian plateau, formed by a collage of microcontinents and arc terranes separated by ophiolitic sutures and which, compared to the Alps or the Himalayas, lacks a prominent axial belt of syn-collisional metamorphic rocks.

6.1. Volcanic and ophiolitic detritus from suture zones

First-cycle detritus from ophiolites, ophiolitic mélanges, arc-related rocks and continental lava fields, widely exposed in eastern Anatolia and along the Zagros suture in Iraq and Iran, represents a significant fraction of Mesopotamian sediments. Provenance from such dense mafic and ultramafic source rocks is readily revealed by high heavy-mineral concentration in sands of the Euphrates River and Mesopotamian floodplain (tHMC 6 ± 3; estimated grain density 2.75 ± 0.04 g/cm^3). Plagioclase/feldspar (P/F) ratios are 82 ± 5 in Euphrates, Tigris and Mesopotamian floodplain sands in central-southern Iraq, and reach above 90 in sands draining volcanic fields or the Erzincan, Bitlis and Zagros suture zones.

In Anatolia, volcanic detritus represented by lathwork to microlitic rock fragments, plagioclase and clinopyroxene, with subordinate hypersthene, oxy-hornblende or olivine, is most common in sands of the Euphrates (Fig. 5D) and its tributaries, especially in the Karasu branch. Uppermost Tigris sand, containing abundant volcanic, metavolcanic and metabasite grains eroded from the Maden Group, is enriched downstream in olivine derived from Plio-Quaternary lavas exposed west of Diyarbakir (Fig. 2). Cellular serpentinite and serpentineschist grains, subordinate in Tigris headwaters draining the Bitlis suture (Sc/S 74 ± 7), are most abundant in upper Karasu sand draining serpentinized harzburgites of the Erzincan suture (Sc/S 49 ± 19), where enstatite, olivine and Cr-spinel are overwhelmed by clinopyroxene derived largely from volcanic rocks. Serpentinite grains, common in Pülümur sands also draining the Erzincan suture (Sc/S 83), are carried by all Anatolian tributaries of the Euphrates and Tigris but the Perisuyu. Enstatite, olivine or Cr-spinel are rare.

In Iraq, volcanic/metavolcanic rock fragments and mainly augitic clinopyroxene characterize the Rawanduz tributary of the Greater Zab, reflecting supply from the Naopurdan-Walash Group (Fig. 3). Low-grade metavolcanic rocks of the Zagros suture supply abundant epidote, widespread in Neogene sandstones as in modern sands recycled from them (Philip, 1968; Ghazal, 2005), along with minor prehnite and pumpellyite commonly detected in Mesopotamian sands. Dominant actinolitic amphibole and hornblende are associated with almost invariably subordinate and generally minor clinopyroxene and rare hypersthene in sands of the Lesser Zab upstream of Lake

Dukan and of its tributaries draining the ophiolitic suture zone, reflecting extensive uralitization in metabasite and gabbroic source rocks (Al-Saffi et al., 2012). Despite of only low-grade metamorphism, amphibole color indices are higher in Mesopotamian sands (HCI 25 ± 10) than generally found in foreland basin sediments (e.g., 8 ± 3, 9 ± 3 and 10 ± 4 for Indus, Ganga and Brahmaputra sands; Garzanti et al., 2005; 2010) because greenish actinolite and blue-green hornblende derived from metavolcanic and retrogressed gabbroic rocks are invariably associated with green-brown kaersutite and reddish-brown oxy-hornblende derived from arc lavas.

The Qara Cholan River and its right-bank tributaries draining the suture zone in Iraq carry mostly lithic to feldspatho-lithic sands locally dominated by metabasite grains (mostly amphibolite, associated with epidosite, metagabbro and chloritoschist; MI up to 403) and containing common volcanic and metavolcanic grains (lathwork, microlitic, metadiabase). Shale/siltstone to slate/metasiltstone, limestone and chert grains derived from sedimentary rocks of the imbricate belt (Qulqula-Khwakurk and Balambo-Tanjero zones) are also common. Plagioclase is the dominant feldspar (P/F 97 ± 5). Ultramafic grains are subordinate even in streams draining almost exclusively the Penjween and Mawat ophiolites. Cellular serpentinite predominates over serpentineschist (Sc/S 87 ± 12) and olivine-bearing peridotite grains occur and are traced to the Lesser Zab downstream. Very rich to extremely rich heavy-mineral assemblages are dominated by amphibole associated with epidote. Clinopyroxene is abundant only locally and hypersthene occurs in detritus from the Penjween Ophiolite. Cr-spinel and olivine are rare, and enstatite very rare. Amphibole-epidote suites shed by the Penjween and Mawat ophiolites contrast with pyroxene suites shed by ophiolitic complexes exposed all along the Alpine-Himalayan belt from the Apennines to the Andaman Islands (Garzanti et al., 2000, 2002a, 2002b, 2013b), reflecting extensive post-obduction greenschist-facies metamorphism of dominantly crustal protoliths.

In Iran, Sirwan sand downstream of the Zagros suture is notably enriched in chert, but not significantly in volcanic or metavolcanic rock fragments; heavy-mineral suites are clinopyroxene-dominated and hypersthene and olivine are present, but heavy-mineral concentration is lower. Jamishan sand draining the Kermanshah Ophiolite is moderately rich in lathwork and subordinately microlitic and metavolcanic rock fragments, contains abundant clinopyroxene but virtually lacks ultramafic detritus. Seymareh sand downstream of the suture is markedly enriched in chert, includes a few serpentinite, enstatite and Cr-spinel grains, but not much volcanic detritus. Volcanic and ultramafic rock fragments are minor in Dez sand, which is very rich in chert and contains clinopyroxene and a little enstatite.

Ultramafic detritus thus notably decreases from eastern Anatolia to Iraqi Kurdistan, and is scarce in Iran (Table 1). Mantle source rocks belonged to the oceanic upper plate obducted onto Arabia in the

Late Cretaceous, and thus cellular serpentinite grains prevail over serpentineschist throughout the Euphrates and Tigris catchments (Fig. 5B; Sc/S 74 ± 14). The Sc/s ratio is mainly in the same range as in sands eroded from other ophiolitic complexes of the "*croissant ophiolitique peri-Arabe*" (Baer Bassit, Kizildag, Mersin and Sama'il ophiolites of Syria, Turkey and Oman; Ricou, 1971), where it ranges between 76 ± 10 and 85 ± 9 (fig. 9 in Garzanti et al., 2002a). Locally lower Sc/S ratio is ascribed to strong post-obduction deformation during Paleogene collision and final Neogene welding between Arabia and Eurasia.

6.2. Metamorphic detritus from axial belts

The best example of an axial neometamorphic complex in the Anatolia-Zagros orogen is the Bitlis-Pütürge massif, exposing greenschist, blueschist and amphibolite-facies rocks with eclogite relics (Oberhänsli et al., 2010). The massif is drained by the Batman, the only major river in our study that carries metamorphiclastic sand (MI 304; Fig. 5A). Downstream of the Batman confluence, Tigris sand is dominated by quartz, granitoid and metamorphic rock fragments, a drastic compositional change testifying to notably higher erosion rates in the Bitlis massif than elsewhere in southeast Anatolia. Medium/high-rank gneiss and amphibolite rock fragments derived from the Bitlis-Pütürge massif are traced to Iraq in Euphrates, Tigris and Mesopotamian floodplain sands. The low-grade neometamorphic basement of the Tauride microcontinent (Malatya-Keban unit) supplies micaschist grains and biotite, most common in Munzur sand.

High-pressure metamorphic rocks are almost lacking in the Zagros orogen (Agard et al., 2005), where the axial belt is represented by the Sanandaj-Sirjan zone affected by very low to low-grade metamorphism only. Sand is thus dominated by sedimentary/metasedimentary and volcanic/metavolcanic detritus (MI* 136 ± 21), with moderately poor to very rich heavy-mineral suites dominated by epidote, amphibole and clinopyroxene. Lower-amphibolite facies conditions were reached in the metamorphic Qandil volcano-sedimentary sequence, and temperatures ≥ 600°C are inferred for contact aureoles surrounding the Bulfat and Penjween gabbros (Jassim and Goff, 2006 p.219-225). Medium to high-rank metamorphic detritus is thus markedly higher along the Lesser Zab upstream of Lake Dukan, where andalusite is abundant. Downstream of Lake Dukan, metamorphic detritus has been diluted, but andalusite is traced to the Tigris confluence. Andalusite, present also in Tigris and Batman sands in Anatolia, occurs in significant amounts in Sirwan and Seymareh sands downstream of the Zagros suture, and is traced all along the Karkheh River as well as from the Dez tributary along the Karun River to the Shatt al-Arab. The HCI index approaches middle amphibolite-facies values in Batman sand (13), and is < 5 in metamorphic detritus elsewhere.

6.3. Sedimentary detritus from the external belt

Because the very thick Phanerozoic succession of the Arabian platform was detached along the underlying Neoproterozoic-Cambrian salt from its basement, the Zagros fold-belt entirely consists of cover strata (Alavi, 2004). Sedimentary detritus consequently represents the major component of the Mesopotamian foreland-basin fill. Sedimentary to very low-rank metasedimentary rock fragments increase markedly in abundance from west to east, being common in Euphrates sand (20 ± 5% of the bulk sample), very common in Tigris sand (42 ± 3%), and overwhelming in Karun and Shatt al-Arab sands (83 ± 7%). The inverse trend is displayed by heavy-mineral concentration, which decreases by an order of magnitude from Euphrates and Tigris sands to Karun and Shatt al-Arab sands, reflecting marked eastward decrease in the exposure of, and hence supply from igneous and metamorphic rocks yielding heavy minerals in significant quantities.

Limestone grains, associated with chert, mudrock and dolostone grains in varying abundance, are predominant (Fig. 5F,I). Such a carbonaticlastic-cherticlastic signature characterizes detritus derived from sedimentary successions deposited originally along the distal passive margin of southern Neotethys (e.g., Hawasina units of northern Oman, Mamonia complex of Cyprus, Toscana-Umbria domain of the Apennines; Garzanti et al., 2000; 2002a; 2002b), where arid/semiarid climate at tropical latitudes since the close of the Paleozoic have favored biogenic carbonate factories rather than physical siliciclastic production. Interbedded quartz-rich sandstones, characteristic of many passive-margin settings (Garzanti et al., 2014), are consequently few, and modern sands are quartz-poor with ZTR ≤ 12 even where entirely derived from sedimentary rocks (e.g., upper Karun). After orogenic accretion into the Alpine-Himalayan belt, carbonate rocks are now widely exposed from the Mediterranean region to central Asia in cold-mountain or still arid/semiarid climates, where chemical weathering is ineffective and soluble limestone clasts, traditionally held to be non-durable, are preserved in abundance (Zuffa, 1985; Garzanti et al., 2005; 2006). Even most labile gypsum grains, associated with very unusual celestite-dominated heavy-mineral assemblages and derived from evaporites of the lower Miocene Gachsaran Formation, are abundant locally in Karkheh sand.

6.4. Recycling of orogen-derived clastic wedges

Quantifying recycling is one of the most difficult tasks in provenance studies of sand and sandstone. Because Mesopotamian sand is almost invariably quartz-poor and dominated by unstable grains, the temptation would be to jump to the very wrong conclusion that they are dominantly first-cycle. Recycling does not necessarily result in concentrating quartz relative to sedimentary source rocks

(Cavazza et al., 1993; Garzanti et al., 2013b), especially in arid climates where weathering is negligible. Not only durable chert, but also unstable carbonate grains, mafic lithics and heavy minerals are recycled in abundance from molassic units of the foothills, as documented in sands of the Aqsu River and middle-course Lesser Zab tributary draining Cenozoic units exclusively (Fig. 5C). Volcanic rock fragments, negligible in Lesser Zab sand upstream of Lake Dukan, increase in abundance as the river cuts across Cenozoic clastic rocks downstream. Epidote dominates transparent heavy-mineral suites in Neogene clastic wedges and river sands recycled from them (Philip, 1968).

A way to determine which minerals are preferentially recycled from Neogene sandstones of the Zagros foothills is to check whether they correlate negatively with the tHMC index in our samples (Fig. 8). Correlations are negative for epidote and durable zircon, tourmaline, rutile and Cr-spinel ($r \approx -0.5$, sign. lev. 0.1%) and poorly negative for apatite, garnet and staurolite ($r \approx -0.3$). Amphibole and pyroxene correlate positively (r 0.3-0.6), and are virtually absent in epidote-dominated recycled sands of the Adhaim-Aqsu River. However, even unstable ferromagnesian minerals can be recycled, because they resisted diagenetic dissolution to some degree (Al-Juboury, 2009) and are quite common in upper Miocene foreland strata drained by the Euphrates (Philip, 1968). This points to decreasing intensity of diagenetic dissolution from more deeply buried internal units of the foothills, containing dominant epidote because ferromagnesian minerals have been selectively dissolved, to foreland strata where diagenetic effects are least extensive and ferromagnesian minerals largely preserved. Virtually full preservation of epidote is indicated by ZTR ≤ 2 in sands of the Aqsu River and middle-course Lesser Zab tributary. In the Lesser Zab, the P/F ratio decreases from 72-88 to 60-67 downstream, and is lowest in Aqsu sand (50) suggesting faster dissolution for plagioclase than for K-feldspar during diagenesis of clastic parent rocks.

A useful tracer of recycling is Cr-spinel (fig. 3 in Garzanti and Andó, 2007a), widespread in Mesopotamian sands and derived ultimately from mafic/ultramafic rocks of the suture zone (Aswad et al. 2011). The relative abundance of Cr-spinel is less in tributaries draining ophiolitic sutures and in Euphrates and Tigris sands ($\leq$ 1%, 1 ± 1% and 2 ± 1% of transparent heavy minerals, respectively) than in tributaries draining Cenozoic strata only and in the Karun River (5 ± 5% and 10 ± 6%, respectively), increases in inverse proportion to transparent-heavy-mineral concentration, and correlates negatively with ultramafic grains (Fig. 8). This confirms that Cr-spinel is largely recycled rather than first cycle (fig. 9 in Garzanti et al., 2013b), and was concentrated by selective diagenetic dissolution of ferromagnesian minerals in Cenozoic clastic parent rocks (Al-Juboury et al., 2009b).

6.5. Polycyclic detritus from the cratonic foreland

Foreland-basin strata are not entirely derived from associated orogens. As the Indo-Gangetic plain is partly fed from right-bank tributaries of the Ganga River draining the Indian shield, so the Mesopotamian basin receives detritus recycled from sedimentary cover of the Arabian foreland in the southwest, consisting of quartzose sand with poor transparent-heavy-mineral suites nearly half of which is zircon, tourmaline and rutile. This additional contribution is distinguished readily by marked local enrichment in coarser and rounded monocrystalline quartz grains, associated with a slight increase in ZTR index and lower P/F in Mesopotamian floodplain sand west of the Euphrates (Fig. 5H), and to a lesser extent in Tigris sand and aeolian dunes west of the Tigris in central Iraq.

A major source of quartzose polycyclic detritus is the Neogene Dibdibba Formation of southern Iraq and Kuwait. These alluvial-fan to deltaic sediments were fed by seasonal floods of a powerful paleo-river flowing along the presently dry Wadi al-Batin and connected with Wadi Rimah of central Arabia during wetter climatic stages (Holm, 1960; Al-Sulaimi and Pitty, 1995). Similar Neogene deposits are patchily exposed along the northeastern margin of the Arabian foreland from Syria to the Gulf (Jassim and Goff, 2006 p.181-183; Al-Juboury, 2009). Additionally, fine-grained quartzose sediment with K-feldspar, zircon and tourmaline is blown during major dust storms from Arabian deserts to reach the Mesopotamian plain, the Gulf and beyond (Fig. 1C; Emery, 1956; Awadh, 2012). This is documented by decrease in P/F from Karun sands (74 ± 7) to Shatt al-Arab sands at Khorramshahr (54 ± 7), where values approach those of Kuwait beach and Wadi al-Batin sands (Table 1).

6.6. Relative sediment contributions

The Euphrates and Tigris rivers drain different geological domains in different proportions, but largely within the same Anatolia-Zagros orogen. The compositional signatures of their sediments thus differ, but not markedly (Fig. 6), and distinguishing their relative contributions to the Mesopotamian foreland basin is not straightforward. The Euphrates carries more detritus from Anatolian volcanic fields (plagioclase, volcanic rock fragments, clinopyroxene and hypersthene; Fig. 5D), the Tigris more sedimentary detritus from the Zagros fold-belt (carbonate, shale/slate, chert) and thus fewer heavy minerals including more zircon, tourmaline, rutile and garnet (Fig. 5E). Instead, dominantly sedimentaclastic sand is carried by the Karun River (Fig. 5F). Forward end-member modelling of integrated petrographic and heavy-mineral data (Garzanti et al., 2012) suggests locally variable but overall similar relative contributions to Mesopotamian sands from the Euphrates (54 ± 35%) and Tigris rivers (45 ± 35%). Quartzose sand from the Arabian foreland,

negligible in the east, represents as much as ~63% and ~82% of the two sand samples collected near Karbala west of the Euphrates.

Greater compositional similarity of Euphrates sand with Murat rather than Karasu sand, and of Tigris sand downstream of the Batman confluence with Batman rather than Tigris sand upstream, indicates the Murat and Batman rivers as the major sediment contributors to the two trunk rivers in Anatolia (94 ± 4% and 83 ± 14%, respectively). Shatt al-Arab sand is calculated to be supplied 100% by the Karun River, and the Kuwait beach 93% from the Arabian foreland and 7% from the combined Euphrates-Tigris-Karun drainage system, although the extremely poor heavy-mineral suite has been contributed virtually entirely by the latter because of very low heavy-mineral concentration in Arabian sources.

6.7. Channel profiles and erosion in an undissected orogen

Relief is controlled by several competing factors, including lithology, tectonics and climate (Burbank and Pinter, 1999). High topography may be residual, reflecting the distribution of erosion-resistant rocks, or may result from focused active uplift. Similarly, knickpoints can be associated with sharp lithological boundaries or active faults. The quantitative analysis of stream profiles is one effective way to characterize a tectonically active mountain region with morphometric parameters that help us investigate the drivers of erosional evolution. Two indices, channel steepness k_s and concavity θ, are defined by a power-law relationship between the local channel slope S and the contributing drainage area A used as a proxy for discharge ($S = k_s A^{-\theta}$; Flint 1974). In this study, the steepness index k_{sn} referenced to a fixed concavity 0.45 (Korup and Schlunegger, 2009) is used to compare gradients in channels with different drainage areas.

We have calculated concavity and steepness indices for 16 short stream segments, draining each a single tectonic unit of the Anatolia-Zagros orogen (Fig. 9). In this broad tectonic domain steepness indices are among the lowest in active orogenic areas, comparable to those in the Apennines (Kirby and Whipple, 2012). Low erosion potential is confirmed by sediment yields and erosion rates around 100 ton/km^2·a and 0.04 mm/a calculated for the entire Euphrates-Tigris basin, increasing to 200-400 ton/km^2·a for the northern mountains facing the Black Sea (Jaoshvili, 2002). Average erosion rates in the Anatolian plateau do not exceed 0.1 mm/a.

Short streams draining the resistant mantle rocks of the Refahiye Ophiolite are steepest and may show extreme concavity, whereas streams draining Neogene volcanic fields or the Kermanshah Ophiolite where volcanic rocks are dominant have low steepness and moderate concavity. Relief thus appears to be controlled more by lithological contrast than by tectonic uplift. Low steepness also characterizes rivers in the Sanandaj-Sirjan zone, with concavities ranging from moderate for

streams draining across structural strike to low or even markedly negative (-0.3) for the Gavrud River draining subparallel to structural strike. The marked change in detrital modes of Sirwan sand across the Zagros suture points to notably low erosion rates in upstream reaches.

Very different morphometry characterizes channels incised into the northern and southern flanks of the Bitlis Massif. The former have gentle profiles with very high concavity, the latter are steeper with moderate concavity (Fig. 9). Channel steepness and erosion rates are relatively high along the southern flank of the Bitlis Massif, but still markedly lower than along Alpine or Himalayan neometamorphic axial belts (Wobus et al., 2003; Korup and Schlunegger, 2009).

7. The use and misuse of provenance models

Foreland-basin sediments conveyed through the Euphrates-Tigris-Karun fluvial network present a unique case of virtually unweathered detritus generated in semiarid climate from a slowly eroding, largely undissected composite orogen produced by ophiolite obduction followed by continental collision. In this section we examine to what extent the lesson learned from our modern-sand perspective may be applicable to the analysis of an imaginary non-diagenetically altered ancient clastic wedge generated by analogous geodynamic processes, and discuss the insight gained and potential pitfalls associated with the classical approach postulating the existence of a direct link between sediment composition and plate-tectonic setting (Dickinson, 1985), versus an upgraded approach focusing specifically on the tectono-stratigraphic level of source terranes (Garzanti, 2016).

7.1. The Dickinson model at work

In the classical triangular diagrams of Dickinson and Suczek (1979), detrital modes of Karun and Tigris sands plot broadly correctly within or at the boundary of the "recycled orogen" field, whereas Euphrates and most Mesopotamian sands straddle that boundary and plot largely in the "magmatic arc" field (Fig. 10). If a provenance diagnosis had to be made for an analogous ancient sandstone suite based on such information alone, then we should be able to infer an active-margin orogenic setting. A fold-thrust/suture belt provenance may be indicated correctly, but it would be hard to tell whether an arc was active at the time of deposition or long extinct, and to establish conclusively that these sediments were deposited in a foreland basin and not for instance in a forearc basin. Carbonate lithics, which may occur in forearc basins although hardly in such abundance (Marsaglia and Ingersoll, 1992; Garzanti et al., 1996; An et al., 2014), would represent a revealing parameter, but they are not considered in the Dickinson (1985) model. The quartz-rich composition of the two

Mesopotamian samples plotting in the "continental block" field may be interpreted correctly as fed mainly from the cratonic foreland.

7.2. The upgraded model at work

The simplest model of a collision orogen includes five types of allochthonous tectonic domains (Garzanti et al., 2007): (1) arc remnants and (2) obducted or accreted ophiolites exposed along the suture zone, (3) an axial belt of high-pressure neometamorphic basement and cover rocks ("fossil continental-subduction zone"), (4) external fold-thrust belts of accreted continental-margin paleometamorphic basement and cover strata, and (5) molassic wedges of the foothills. Orogenic sediments can thus be envisaged as mixtures in various proportions of such five sources (magmatic arc, ophiolite, axial belt, continental block, and recycled clastic provenances). Each domain but the fifth can be idealized as a tectono-stratigraphic multilayer evolving progressively while erosion cuts deeper from the shallow supracrustal to the deep crustal or even mantle level. Undissected, transitional and dissected stages can thus be defined for each provenance but the fifth, and traced in space or time by their distinct petrographic and mineralogical fingerprints.

Sand eroded from the Anatolia-Zagros orogen is significantly richer in sedimentary/low-rank metasedimentary and volcanic/low-rank metavolcanic lithics and much poorer in quartz, K-feldspar and high-rank metamorphic detritus than sand generated along the Alpine-Himalayan system (Fig. 11). Besides the classic amphibole-epidote-garnet orogenic triad (Garzanti and Andó, 2007b), heavy-mineral suites in the Anatolia-Zagros orogen include invariably abundant and even dominant clinopyroxene commonly associated with some hypersthene. In an imaginary ancient analog, such signatures would lead us to infer deposition in a foreland basin by rivers draining within the external fold-thrust belt and across volcanic-arc rocks and ophiolites of the suture zone. The dearth of high-rank metamorphic detritus would indicate dominance of supracrustal tectono-stratigraphic levels across the orogenic source, with minor exposures of a neometamorphic axial belt and/or paleometamorphic basement. It would not be difficult to figure out that carbonaticlastic/cherticlastic detritus was supplied in arid climatic conditions from strata originally deposited on the distal continental-margin of the lower plate and subsequently accreted at the front of the outward-growing accretionary prism. The existence of a tectonic detachment above the basement of the lower-plate continental margin with accretion of cover strata in mainly thin-skinned mode could be guessed. The paleovolcanic nature of most arc sources would be readily inferred from the abundance of very-low-rank metavolcanic grains and low-grade minerals (i.e., epidote with minor prehnite and pumpellyite). Predominant cellular serpentinite grains would reveal the original upper-plate setting of ophiolitic source rocks. The abundance of actinolite-rich rock fragments and very rich

amphibole-epidote heavy-mineral suites would suggest dominance of crustal over mantle protoliths in the originally obducted ophiolitic allochthons and regional post-obduction greenschist-facies metamorphism.

Sediments derived from undissected collision orogens such as the wide Anatolia-Zagros plateau share all of their main diagnostic compositional signatures with detritus from singly-vergent thin-skinned thrust belts such as the Apennines (Garzanti et al., 2002b), and thus the geometry of subduction could not be inferred. Although the Amazon River carries a similar pyroxene-rich heavy-mineral suite as the Euphrates (Limonta et al., 2015), Mesopotamian sediments are readily distinguished from those shed from either side of an Andean-type cordillera. The feldspatho-lithic volcaniclastic to litho-quartzo-feldspathic plutoniclastic signatures of magmatic arc provenance characterize the Pacific side of the Andes (Yerino and Maynard 1984; Thornburg and Kulm 1987), whereas litho-quartzose to quartzose metamorphiclastic sand lacking carbonate and ultramafic grains characterize its retro-side (DeCelles and Hertel, 1989; Johnsson et al., 1991). Carbonate grains shed from Laramide uplifts are however found in abundance locally in syn-orogenic clastic wedges of the Rocky Mountain foreland basin (Ingersoll et al., 1987).

The most challenging problem is posed by detritus recycled along both flanks of the foreland basin. Local addition of quartzose detritus recycled from siliciclastic cover rocks of the cratonic foreland would be easier to appraise, but it would be hard not to underestimate the amount of unstable carbonate, mafic/ultramafic rock fragments, epidote and other heavy minerals recycled from molassic units of the foothills (Fig. 5C). The widespread occurrence of Cr-spinel would offer the best evidence for the largely recycled origin of ultramafic detritus, rather than first-cycle provenance from ophiolitic allochthons.

8. Long-distance sediment dispersal in arid climate

Because of arid climate and consequently limited river-transport capacity, the Arabian/Persian Gulf is presently underfilled and dominated by carbonate sedimentation despite the existence of a major longitudinal river system and transverse rivers draining the Zagros Mountains in southern Iran (Baltzer and Purser, 1990; Kendall and Alsharhan, 2010). During the major eustatic lowstands of the Pleistocene, however, the Gulf was overfilled and subaerial, and trunk-river sediments reached into the Gulf of Oman remnant-ocean basin (Lambeck, 1996; Uchupi et al., 1999). Loose sediments of the floodplain were then deflated by reinforced northerly (Shamal) winds, and eventually pushed southwestwards onto Arabia where they accumulated in vast dunefields (Glennie and Singhvi, 2002).

By combining petrographic, mineralogical and geochronological fingerprints we can trace sediment dispersal from the Anatolia-Zagros orogen to as far as the heart of Arabia. In this long multistep transport process, finer-grained quartz-poor orogenic sand from the north has mixed with coarser-grained quartz-rich sand recycled from lower Paleozoic and younger quartzarenites overlying and surrounding the Neoproterozoic Arabian shield in the west. This has occurred first locally along the western foreland side of the Mesopotamian floodplain (Fig. 5H), and next along the western shores of the Gulf. Orogenic detritus is estimated to represent ~40% of eolian sand in the coastal Jafurah dunefield of eastern Saudi Arabia (decreasing from 65 ± 25% in very fine sand to 5 ± 5% in medium sand; fig. 7 in Garzanti et al., 2013a). Composition changes progressively inland, and orogenic detritus decreases to virtually 0% in western Jafurah dunes, which largely consist of polycyclic quartzose sand deflated from the Dibdibba plains of Kuwait. Jafurah dunes contain a few zircon grains yielding Paleogene, Late Cretaceous, Jurassic or Permian ages (fig. 9 in Garzanti et al., 2013a), which are not documented in Arabia but are common in Mesopotamian river sands, thus confirming minor sediment contribution from the latter.

Identical feldspatho-litho-quartzose carbonaticlastic compositions revealing mixing in subequal proportions of quartz-poor orogenic and quartz-rich anorogenic sands are traced southward along the western shores of the Gulf from north of Dammam to coastal Jafurah dunes and as far as inland Sabkha Matti at the edge of the Rub'al-Khali desert (Fig. 1C). In contrast, coastal dunes in the United Arab Emirates are lithic carbonaticlastic with epidote-rich heavy-mineral assemblages, indicating recycling of Pleistocene eolianites and ultimate provenance largely from the Zagros fold-belt in the north (Garzanti et al., 2003). Quartz increases rapidly inland, but orogenic detritus remains common in litho-feldspatho-quartzose dune sand of the Liwa oasis (fig. 8 in Garzanti et al., 2013a). The orogenic trace fades in feldspatho-quartzose Rub'al-Khali megadunes of Saudi Arabia, which contain a few chert, volcanic, carbonate, low-rank metabasite and ultramafic grains. Sand grains have thus traveled by multistep fluvial and eolian transport a distance up to ~4000 km, from the Euphrates headwaters to the Rub'al-Khali sand sea.

9. Conclusions

The Anatolia-Zagros orogen chiefly includes remnants of magmatic arcs, obducted ophiolites and a frontal fold-thrust belt of thick sedimentary strata. Paleometamorphic basement is virtually lacking. Subducted continental crust with high-pressure neometamorphic overprint is exposed in the Bitlis-Pütürge massif of southern Anatolia but not in the Zagros Mountains of Iran, where the axial belt is represented by the Sanandaj-Sirjan zone affected by very low to low-grade metamorphism only. These features are reflected by markedly distinct petrographic and heavy-mineral signatures of

sediments generated across the entire Anatolia-Iranian plateau relative to foreland-basin sediment derived from the Alps or the Himalayas, and represent the distinctive detrital fingerprint of this type of broad and composite, slowly eroding undissected orogenic domain. Lithic-rich detritus from supracrustal rocks including carbonates, cherts, arc lavas, oceanic mélanges and obducted ophiolitic allochthons dominates over quartz, K-feldspar, high-rank metamorphic rock fragments and mica. Pyroxene is nearly as abundant as amphibole or epidote, and much more common than any other heavy mineral; andalusite is the only locally significant heavy mineral derived from medium-grade metasedimentary rocks. Because chemical weathering is negligible in arid climates, even soluble gypsum grains may be locally abundant, and carbonate rock fragments are preserved through multiple sedimentary cycles. Recycling of Neogene molasse produces lithic sand characterized by abundant carbonate and mafic volcanic rock fragments (Fig. 5C), with epidote-dominated heavy-mineral suites that include Cr-spinel and a few amphibole and pyroxene grains. Recycling does not necessarily produce "*mature*" daughter sediments with more quartz, zircon, tourmaline or rutile than in parent rocks. Relative enrichment in K-feldspar and epidote in recycled sands points to selective diagenetic dissolution of plagioclase and ferromagnesian minerals in Neogene units of the Zagros foothills.

In contrast to foreland basins associated with highly elevated, fast-eroding and deeply dissected collision orogens such as the Himalaya, the Zagros foreland basin is presently underfilled. The Mesopotamian plains pass southeastward, through a marshland where sediments of the Euphrates and Tigris Rivers are dumped, to the shallow sea of the Arabian/Persian Gulf dominated by allochemical carbonate sedimentation. The quartz-poor orogenic signature of sediments derived from eastern Anatolia, Iraq and Iran, progressively diluted by mixing with quartz-rich anorogenic sand recycled from siliciclastic units of Arabia, can be traced along the southwestern side of the Gulf to the Rub' al-Khali sand sea. This modern-sand provenance study highlights the diversity of plate-tectonic settings and associated long-distance and multistep source-to-sink sediment-routing systems found in nature, and potential pitfalls encountered when reconstructing past orogenic landscapes without suitable provenance models.

ACKNOWLEDGMENTS

Awaz Kareem Rasul, Waleed Sulaiman Aswad, Ali Daoud, Nawrast Sabah Abdulwahab, Usama Qasim Khaleefah, Dawood Wali and James Howard helped us to obtain additional samples from scarcely accessible areas of war-troubled Iraq. Luca Caracciolo kindly collected the Kuwait beach sand. George Peters helped with the U-Pb analyses. PV was financially supported by a ERC

Starting Grant 259504 ('KarSD'). Very careful review and editing by Ray Ingersoll is very gratefully acknowledged.

SUPPLEMENTARY MATERIAL

Supplementary data associated with this article can be found in the online version, at http://dx.doi._____. These include information on sampling sites (Table A1), the complete bulk-sand petrography (Table A2), heavy-mineral (Table A3), geochemical (Table A4) and geochronological datasets (Table A5), a compilation of published geochronological data in source rocks of the Anatolia-Zagros orogen (Table A6), and morphological parameters of studied river tracts (Table A7). The Google-Earth map of sampling sites *EuTiKa.kmz* is also provided.

FIGURES

Figure 1. Shaded relief map of the Euphrates-Tigris-Karun drainage basin with sample location (**A**; modified after Partow, 2001). **B**) Imaginary reconstruction of river drainage in the "Garden of Eden", as described in the Genesis of the Bible. **C**) Dust storm carrying Arabian dust to Mesopotamia and the Gulf.

Figure 2. Geology of eastern Anatolia (redrawn after the Geological Map of Turkey 1:2,000,000; location within the Euphrates-Tigris-Karun basin shown in inset, drainage divide outlined by thick grey line), illustrating bedrock units exposed in the headwaters of the Euphrates and Tigris Rivers.

Figure 3. Geology of the Iraqi Kurdistan region (redrawn after the Lithostratigraphic Map of northern Iraq; location within the Euphrates-Tigris-Karun basin shown in inset), illustrating bedrock units exposed in the diverse tectonic domains drained by Zagros tributaries of the Tigris River. Gabbroic massifs: Bu = Bulfat; Ma = Mawat; Pe = Penjween; Pu = Pushtashan.

Figure 4. Geology of the central Zagros orogen (redrawn after the Geological Map of Iran 1:2,500,000; location within the Euphrates-Tigris-Karun basin shown in inset), illustrating bedrock units exposed in the diverse tectonic domains drained by the Karun, Karkheh and Sirwan (Diyala) Rivers.

Figure 5. Petrography of Euphrates-Tigris-Karun river sands. **Orogenic provenances**: **A**) Metamorphiclastic detritus from the Bitlis massif (M = metamorphic lithic; m = mica). **B**) Cellular serpentinite (Sc) and foliated serpentineschist (Ss) grains from ophiolites of the Zagros suture. **C**) Volcanic (V), chert (H) and carbonate (C) grains recyled entirely from Neogene molasse units of the foothills. **Trunk-river systems**: **D**) Euphrates sand rich in volcanic detritus including plagioclase (P) and clinopyroxene (p). (**E**) Tigris sand rich in sedimentary detritus (S = shale lithic; e = epidote). **F**) Carbonaticlastic Karun sand. **Foreland-basin fill**: **G**) Mesopotamian sediments derived from Euphrates and Tigris Rivers in subequal proportions. **H**) Rounded quartz grains (Q) recycled from Arabian sources mixed with finer-grained quartz-poor orogenic detritus in the Karbala area (calcareous grains stained with alizarine red). **I**) Carbonaticlastic Shatt al-Arab sand supplied entirely by the Karun River because Euphrates and Tigris bedload is trapped in Iraqi marshlands before reaching the Gulf. All photos with crossed polars; all blue bars for scale are 250 μm.

Figure 6. Detrital modes and heavy-mineral suites in Mesopotamian foreland-basin sediments are intermediate between Euphrates and Tigris sands. Euphrates supply predominates in the northwest, Tigris contribution in the southeast. Floodplain samples collected west of the Euphrates are locally enriched markedly in quartz, zircon, tourmaline and rutile recycled from siliciclastic units in Arabia. Tigris sands between the Lesser Zab and Adhaim confluences are also enriched in quartz from the Arabian foreland. Q = quartz; F = feldspars; L = lithic grains (Lm = metamorphic; Lv = volcanic; Ls = sedimentary). Amp = amphibole; Px = pyroxene; Ol = olivine; &tHM = other transparent heavy minerals; ZTR = zircon + tourmaline + rutile; Sp = Cr-spinel; Ep = epidote group minerals; Grt = garnet; MM = chloritoid + staurolite + andalusite + kyanite + sillimanite.

Figure 7. U-Pb age spectra of detrital zircons in Euphrates-Tigris-Karun river sands, plotted as Kernel Density Estimates (Vermeesch 2012). We used $^{206}Pb/^{238}U$ and $^{207}Pb/^{206}Pb$ ages for zircons younger and older than 1100 Ma, respectively; n = number of concordant ages. Cumulative age distributions show nearly identical patterns for Karun and Shatt al-Arab zircons, as confirmed by much shorter Kolmogorov-Smirnov distance than for Euphrates and Tigris zircons. All plots generated using software package '*provenance*' (Vermeesch et al., 2016).

Figure 8. Provenance discrimination with the compositional biplot (Gabriel, 1971). Sands of the Mesopotamian foreland basin are a mixture of orogenic detritus derived largely from sedimentary rocks (e.g., accreted to the Zagros fold-belt and drained by the Karun), volcanic arcs and ophiolitic sutures (e.g., drained by Euphrates headwaters), and only subordinately from metamorphic complexes (e.g., Bitlis Massif drained by the Batman tributary of the Tigris). Quartz-rich detritus, supplied from Arabia along the western side of the foreland basin, is overwhelming in Kuwait beach sand. All major petrographic and heavy-mineral parameters are considered, and both multivariate observations (points) and variables (rays) are displayed. The length of each ray is proportional to the variability of the compositional parameter in the data set. If the angle between two rays is close to 0°, 90°, and 180°, then the corresponding parameters are directly correlated, uncorrelated, and inversely correlated, respectively. GSZ = grain size (in μm); KF = K-feldspar; L = lithic grains (Lp = shale/siltstone; Lms = low-rank metasedimentary; Lmf = high-rank felsic metamorphic; Lmb = high-rank metabasite); HMC = Heavy Mineral Concentration; MM = chloritoid + staurolite + andalusite + kyanite + sillimanite). Other parameters as in Table 1.

Figure 9. Results of channel-profile analysis. Fluvial network delineated in TecDEM (software shell implemented in MATLAB; Shahzad and Gloaguen, 2011) from a 30 m resolution digital elevation model provided by ASTER GDEM (http://www.gdem.aster.ersdac.or.jp).

Figure 10. Provenance insights obtained from Dickinson's (1985) diagrams. An active margin setting can be inferred, but sands of the Mesopotamian foreland basin plot in both magmatic arc and recycled orogen fields. Karun sand plots in the recycled orogen field, but most information is lost by neglecting carbonate rock fragments representing the majority (57 ± 8%) of detrital grains. Polycyclic quartz sands derived from the Arabian foreland plot correctly in the continental block field.

Figure 11. Contrasting composition of foreland-basin sands derived from dissected Alpine-Himalayan and undissected Anatolia-Iranian collision orogens. Major rivers draining neometamorphic gneiss domes exposed in the axial Alps or Himalayas carry litho-feldspatho-quartzose metamorphiclastic sand with amphibole-epidote-garnet heavy-mineral suites, whereas the Anatolia-Iranian plateau generates feldspatho-quartzo-lithic sedimentaclastic, volcaniclastic or ophioliticlastic detritus notably richer in pyroxene (data from Garzanti et al., 2005; 2010; 2012; Vezzoli et al., 2014 and own unpublished database). The Miocene Kithrea Flysch is exposed in the Kyrenia Range of north Cyprus. Compositional parameters as in Figure 6. The LmLvLs diagram poorly illustrates level of unroofing because medium/high-grade metamorphic rocks are coarse-grained and thus shed virtually no aphanite lithics.

Table 1. Petrography and mineralogy of Euphrates-Tigris-Karun river sands and Mesopotamian foreland-basin sediments. N° = number of samples;Q = quartz; F = feldspars (P = plagioclase); L = lithic grains (Lvm = volcanic and low-rank metavolcanic; Lc = carbonate; Lh = chert; Lsm = other sedimentary and low-rank metasedimentary; Lm = high-rank metamorphic; Lu = ultramafic); MI = Metamorphic Index; tHMC = transparent Heavy Mineral Concentration; ZTR = zircon + tourmaline + rutile; Ttn = titanite; Ap = apatite; Ep = epidote group minerals; Grt = garnet; And = andalusite; Amp = amphibole; Cpx = clinopyroxene; En = enstatite; Hy = hypersthene; Ol = olivine; Sp = Cr-spinel; &tHM = other transparent heavy minerals (kyanite, staurolite, prehnite, pumpellyite, chloritoid, anatase, brookite, sillimanite, celestite and barite); HCI = Hornblende Color Index.

Table 2. Geochemical composition of Euphrates-Tigris-Karun river sands.

REFERENCES

Afkhami, M., 2003. Environmental effects of salinity in the Karun-Dez basin, Iran. 7th International Water Technology Conference Egypt, p. 229-233.

Agard, P., Omrani, J., Jolivet, L., Mouthereau, F., 2005. Convergence history across Zagros (Iran): constraints from collisional and earlier deformation. International Journal of Earth Sciences, 94, 401-419.

Alavi, M., 1994. Tectonics of the Zagros orogenic belt of Iran: new data and interpretations. Tectonophysics 229, 211-238.

Alavi, M., 2004. Regional stratigraphy of the Zagros fold-thrust belt of Iran and its proforeland evolution. American Journal of Science 304, 1-20.

Ali, J., 1976. Heavy minerals provinces of the recent sediments of Euphrates-Tigris basin. Journal of the Geological Society of Iraq 10, 33-46.

Ali, S.A., Buckman, S., Aswad, K.J., Jones, B.G., Ismail, S.A., Nutman, A.P., 2013. The tectonic evolution of a Neo-Tethyan (Eocene-Oligocene) island-arc (Walash and Naopurdan groups) in the Kurdistan region of the Northeast Iraqi Zagros Suture Zone. Island Arc 22, 104-125.

Al-Juboury, A.I., 2009. The Upper Miocene Injana (Upper Fars) Formation of Iraq: insights on provenance history. Arabian Journal of Geosciences 2, 337-364.

Al-Juboury, A.I., Al-Hadidy, A.H., 2009. Petrology and depositional evolution of the Paleozoic rocks of Iraq. Marine and Petroleum Geology 26, 208-231.

Al-Juboury, A.I., Al-Miamary, F.A., 2009. Geochemical variations in heavy minerals as provenance indications: application to the Tigris river sand, northern Iraq. Journal of Mediterranean Earth Sciences 1, 33-45.

Al-Juboury, A.I., McCann, T., 2008. The Middle Miocene Fatha (Lower Fars) Formation of Iraq. GeoArabia 13, 141-174.

Al-Juboury, A.I., Ghazal, M., McCann, T., 2009a. Provenance of Miocene sandstones in northern Iraq: constraints from framework petrography, bulk-rock geochemistry and mineral chemistry. Russian Journal of Geology and Geophysics 50, 517-534.

Al-Juboury, A.I., Ghazal, M., McCann, T., 2009b. Detrital chromian spinels from Miocene and Holocene sediments of northern Iraq: provenance implications. Journal of Geosciences, Czech Geological Survey 54, 289–300.

Allen, M.B., Saville, C., Blanc, E.J.-P., Talebian, M., Nissen, E., 2013. Orogenic plateau growth: expansion of the Turkish-Iranian Plateau across the Zagros fold-and-thrust belt. Tectonics 32, 171-190.

Al-Saffi, I.K., Hadi, A., Aqrawi, A.M.A., 2012. Petrology of gabbroic rocks of Mawat Ophiolite Complex (central sector), NE Iraq. Iraqi Bulletin of Geology and Mining 8, 65-85.

Al-Sulaimi, J.S., Pitty, A.F., 1995. Origin and depositional model of Wadi Al-Batin and its associated alluvial fan, Saudi Arabia and Kuwait. Sedimentary Geology 97, 203-229.

An, W., Hu, X., Garzanti, E., BouDagher-Fadel, M.K., Wang, J., Sun, G., 2014. Xigaze forearc basin revisited (South Tibet): provenance changes and origin of the Xigaze Ophiolite. Geological Society of America Bulletin 126, 1595-1613.

Andó, S., Morton, A., Garzanti, E., 2014. Metamorphic grade of source rocks revealed by chemical fingerprints of detrital amphibole and garnet. Geological Society London, Special Publications 386, 351-371.

Angiolini, L., Balini, M., Garzanti, E., Nicora, A., Tintori, A., Crasquin, S., Muttoni, G., 2003. Permian climatic and paleogeographic changes in Northern Gondwana: the Khuff Formation of Interior Oman. Palaeogeography, Palaeoclimatology, Palaeoecology 191, 269-300.

Aqrawi, A.A.M., 1994. Petrography and mineral content of sea-floor sediments of the Tigris-Euphrates Delta, North-west Arabian Gulf, Iraq. Estuarine, Coastal and Shelf Science 38, 569-582.

Aqrawi, A.A.M., Evans, G., 1994. Sedimentation in the lakes and marshes (Ahwar) of the Tigris–Euphrates delta, southern Mesopotamia. Sedimentology 41, 755-776.

Arfania, R., Shahriari, S., 2009. Role of southeastern Sanandaj–Sirjan Zone in the tectonic evolution of Zagros Orogenic Belt, Iran. Island Arc 18, 555-576.

Aswad, K.J., Aziz, N.R., Koyi, H.A., 2011. Cr-spinel compositions in serpentinites and their implications for the petrotectonic history of the Zagros Suture Zone, Kurdistan Region, Iraq. Geological Magazine 148, 802-818.

Awadh, S.M., 2012. Geochemistry and mineralogical composition of the airborne particles of sand dunes and dust storms settled in Iraq and their environmental impacts. Environmental Earth Sciences, 66, 2247. doi:10.1007/s12665-011-1445-6

Awadh, S.M., Ali, M.O., Ali, R.A., 2011. Mineralogy and palynology of the Mesopotamian plain sediments, Central Iraq. Arabian Journal of Geosciences, 4, 1261-1271.

Aziz N.R.H., Aswad, K.J.A., Koyi, H.A., 2011. Contrasting settings of serpentinite bodies in the northwestern Zagros Suture Zone, Kurdistan Region, Iraq. Geological Magazine 148, 819-837.

Bahroudi, A., Koyi, H.A., 2003. Effect of spatial distribution of Hormuz salt on deformation style in the Zagros fold and thrust belt: an analogue modelling approach. Journal of the Geological Society London 160, 719-733.

Baltzer, F., Purser, B.H., 1990. Modern alluvial fan and deltaic sedimentation in a foreland tectonic setting: the lower Mesopotamian plain and the Arabian Gulf. Sedimentary Geology 67, 175-197.

Berry, R.W., Brophy, G.P., Naqash, A., 1970. Mineralogy of the suspended sediment in the Tigris, Euphrates and Shatt Al-Arab rivers of Iraq, and the recent history of the Mesopotamian plain. Journal of Sedimentary Petrology 40, 131-139. Burbank, D.W., Pinter, N., 1999. Landscape evolution: the interactions of tectonics and surface processes. Basin Research 11, 1-6.

Cavazza, W., Zuffa, G.G., Camporesi, C., Ferretti, C., 1993. Sedimentary recycling in a temperate climate drainage basin (Senio River, north-central Italy): composition of source rock, soil profiles, and fluvial deposits. Geological Society of America, Special Papers 284, 247-262.

Cavazza, W., Albino, I., Zattin, M., Galoyan, G., Imamverdiyev, N., Melkonyan, R., 2015. Thermochronometric evidence for Miocene tectonic reactivation of the Sevan–Akera suture zone (Lesser Caucasus): a far-field tectonic effect of the Arabia–Eurasia collision?. Geological Society London, Special Publication 428, SP428-4.

Cullen, H.M., deMenocal, P.B., 2000. North Atlantic influence on Tigris–Euphrates streamflow. International Journal of Climatology, 20, 853-863.

DeCelles, P.G., Hertel, F., 1989. Petrology of fluvial sands from the Amazonian foreland basin, Peru and Bolivia. Geological Society of America Bulletin 101, 1552-1562.

Dercourt, J., Gaetani, M., Vrielynck, B., Barrier, E., Biju-Duval, B., Brunet, M.F., Cadet, J.P., Crasquin, S., Sandulescu, M. (Eds) 2000. Atlas Peri-Tethys, Palaeogeographical Maps. Paris: CCGM, CGMW, 269 p.

Dickinson, W.R., 1985, Interpreting provenance relations from detrital modes of sandstones. In: Zuffa, G.G. (Ed.), Provenance of arenites. Reidel, Dordrecht, Nato ASI Series 148, pp. 333-361.

Dickinson, W.R., Suczek, C.A., 1979. Plate tectonics and sandstone composition. American Association of Petroleum Geologists Bulletin 63, 2164-2172.

Elmas, A., Yilmaz, Y., 2003. Development of an oblique subduction zone - Tectonic evolution of the Tethys suture zone in southeast Turkey. International Geology Review 45, 827-840.

Emery, K.O., 1956. Sediments and water of Persian Gulf. American Association of Petroleum Geologists Bulletin 40, 2354-2383.

Evans, G., 2011. An historical review of the Quaternary sedimentology of the Gulf (Arabian/Persian Gulf) and its geological impact. In: Kendall, C.G.St, Alsharhan, A. (Eds.), Quaternary carbonate and evaporite sedimentary facies and their ancient analogues: a tribute to D.J. Shearman. Wiley-Blackwell, Chichester, International Association of Sedimentologists, Special Pubblication 43, pp. 11-44.

Flint, J.J., 1974. Stream gradient as a function of order, magnitude, and discharge. Water Resources Research 10, 969-973.

Gabriel, K.R., 1971. The biplot graphic display of matrices with application to principal component analysis. Biometrika, 58, 453-467.

Galehouse, J.S., 1971. Point counting. In: Carver, R.E. (Ed.), Procedures in sedimentary petrology. Wiley, New York, pp. 385-407.

Garzanti, E., 2016. From static to dynamic provenance analysis – Sedimentary petrology upgraded. Sedimentary Geology, Sedimentary Geology, 336, 3-13.

Garzanti, E., Andó, S., 2007a. Heavy-mineral concentration in modern sands: implications for provenance interpretation. In: Mange, M.A., Wright, D.T. (Eds.), Heavy Minerals in Use. Elsevier, Amsterdam, Developments in Sedimentology Series 58. pp. 517–545.

Garzanti, E., Andó S., 2007b. Plate tectonics and heavy-mineral suites of modern sands. In: Mange, M.A., Wright, D.T. (Eds.), Heavy Minerals in Use. Elsevier, Amsterdam, Developments in Sedimentology Series 58, pp. 741-763.

Garzanti, E., Resentini, A., 2016. Provenance control on chemical indices of weathering (Taiwan river sands). Sedimentary Geology, 336, 81-95.

Garzanti, E., Vezzoli, G., 2003. A classification of metamorphic grains in sands based on their composition and grade. Journal of Sedimentary Research 73, 830-837.

Garzanti, E., Critelli, S., Ingersoll, R.V., 1996. Paleogeographic and paleotectonic evolution of the Himalayan Range as reflected by detrital modes of Tertiary sandstones and modern sands (Indus transect, India and Pakistan). Geological Society of America Bulletin 108, 631-642.

Garzanti, E., Andó, S., Scutellà, M., 2000. Actualistic ophiolite provenance: the Cyprus Case. The Journal of Geology 108, 199-218.

Garzanti, E., Vezzoli, G., Andó, S., 2002a. Modern sand from obducted ophiolite belts (Oman, U.A.E.). The Journal of Geology 110, 371-391.

Garzanti, E., Canclini, S., Moretti Foggia, F., Petrella, N., 2002b. Unraveling magmatic and orogenic provenances in modern sands: the back-arc side of the Apennine thrust-belt (Italy). Journal of Sedimentary Research 72, 2-17.

Garzanti, E., Andó, S., Vezzoli, G., Dell'Era, D., 2003. From rifted margins to foreland basins: investigating provenance and sediment dispersal across desert Arabia (Oman, UAE). Journal of Sedimentary Research 73, 572-588.

Garzanti, E., Vezzoli, G., Andó, S., Paparella, P., Clift, P.D., 2005. Petrology of Indus River sands: a key to interpret erosion history of the Western Himalayan Syntaxis. Earth and Planetary Science Letters 229, 287-302.

Garzanti, E., Andó, S., Vezzoli, G., 2006. The continental crust as a source of sand (Southern Alps cross-section, Northern Italy). The Journal of Geology 114, 533-554.

Garzanti, E., Doglioni, C., Vezzoli, G., Andó, S., 2007. Orogenic belts and orogenic sediment provenance. The Journal of Geology 115, 315-334.

Garzanti, E., Andó, S., Vezzoli, G., 2009. Grain-size dependence of sediment composition and environmental bias in provenance studies. Earth and Planetary Science Letters 277, 422-432.

Garzanti, E., Andó, S., France-Lanord, C., Vezzoli, G., Najman, Y., 2010. Mineralogical and chemical variability of fluvial sediments. 1. Bedload sand (Ganga-Brahmaputra, Bangladesh). Earth and Planetary Science Letters 299, 368-381.

Garzanti, E., Resentini, A., Vezzoli, G., Andó, S., Malusà, M., Padoan, M., 2012. Forward compositional modelling of Alpine orogenic sediments. Sedimentary Geology 280, 149-164.

Garzanti, E., Vermeesch, P., Andó, S., Vezzoli, G., Valagussa, M., Allen, K., Khadi, K.A., Al-Juboury, I.A., 2013a. Provenance and recycling of Arabian desert sand. Earth-Science Reviews 120, 1-19.

Garzanti, E., Limonta, M., Resentini, A., Bandopadhyay, P.C., Najman, Y., Andó, S., Vezzoli, G. 2013b. Sediment recycling at convergent plate margins (Indo-Burman Ranges and Andaman-Nicobar Ridge). Earth-Science Reviews 123, 113-132.

Garzanti. E., Vermeesch, P., Padoan, M., Resentini, A., Vezzoli, G., Andó, S., 2014. Provenance of passive-margin sand (southern Africa). The Journal of Geology 122, 17-42.

Garzanti, E., Andó, S., Padoan, M., Vezzoli, G., El Kammar, A., 2015. The modern Nile sediment system: processes and products. Quaternary Science Reviews 130, 9-56.

Ghasemi, A., Talbot, C.J., 2006. A new tectonic scenario for the Sanandaj–Sirjan Zone (Iran). Journal of Asian Earth Sciences 26, 683-693.

Ghazal, M.M., 2005. Variation of the modal percentages of epidote in recent sediments from selected localities in northern Iraq. Rafidain Journal of Science, 16, 13-25.

Glennie, K.V., Singhvi, A.K., 2002. Event stratigraphy, paleoenvironment and chronology of SE Arabian deserts. Quaternary Science Reviews 21, 853-869.

Griffin, W.L., Powell, W.J., Pearson, N.J., O'Reilly, S.Y., 2008. GLITTER: data reduction software for laser ablation ICP–MS. In: Sylvester, P. (Ed.), Laser ablation–ICP–MS in the earth sciences: current practices and outstanding issues. Mineralogical Association of Canada Short Course 40, 204-207.

Hessami, K., Koyi, H.A., Talbot, C.J., Tabasi, H., Shabanian, E., 2001. Progressive unconformities within an evolving foreland fold–thrust belt, Zagros Mountains. Journal of the Geological Society 158, 969-981.

Holm, D.A., 1960. Desert geomorphology of the Arabian Peninsula. Science 132, 1369-1379.

Hubert, J.F., 1962. A zircon-tourmaline-rutile maturity index and the interdependence of the composition of heavy mineral assemblages with the gross composition and texture of sandstones. Journal of Sedimentary Petrology, 32, 440-450.

Ingersoll, R.V., 1990. Actualistic sandstone petrofacies: discriminating modern and ancient source rocks. Geology 18, 733-736.

Ingersoll, R.V., Bullard, T.F., Ford, R.L., Grimm, J.P., Pickle, J.D., Sares, S.W., 1984. The effect of grain size on detrital modes: a test of the Gazzi–Dickinson point-counting method. Journal of Sedimentary Petrology 54, 103-116.

Ingersoll, R.V., Cavazza, W., Graham, S.A., 1987. Provenance of impure calclithites in the Laramide foreland of southwestern Montana. Journal of Sedimentary Research 57, 995-1003.

Jaoshvili, S., 2002. The rivers of the Black Sea. European Environmental Agency. Technical report 71, 58 p.

Jassim, S.Z., Goff, J.C., 2006. Geology of Iraq. Dolin, Prague, 341p.

Johnsson, M.J., Stallard, R.F., Lundberg, N., 1991. Controls on the composition of fluvial sands from a tropical weathering environment: sands of the Orinoco River drainage basin, Venezuela and Colombia. Geological Society of America Bulletin 103, 1622-1647.

Jotheri, J., Allen, M.B., Wilkinson, T.J., 2016. Holocene avulsions of the Euphrates River in the Najaf area of western Mesopotamia: impacts on human settlement patterns. Geoarcheology, doi 10.1002/gea.21548.

Kendall, C.G.St, Alsharhan, A., 2010. Quaternary carbonate and evaporite sedimentary facies and their ancient analogues: a tribute to D.J. Shearman. Wiley-Blackwell, Chichester, International Association of Sedimentologists, Special Pubblication 43, 496 p.

Kirby, E., Whipple, K.X., 2012. Expression of active tectonics in erosional landscapes. Journal of Structural Geology, 44, 54-75.

Korup, O., Schlunegger, F., 2009. Rock-type control on erosion-induced uplift, eastern Swiss Alps. Earth and Planetary Science Letters, 278, 278-285.

Lambeck, K., 1996. Shoreline reconstructions for the Persian Gulf since the last glacial maximum. Earth and Planetary Science Letters 142, 43-57.

Lees, G.M., Falcon, N.L., 1952. The geographical history of the Mesopotamian plains. Geographical Journal 118, 24-39.

Limonta, M., Garzanti, E., Resentini, A., Andó, S., Boni, M., Bechstädt, T., 2015. Multicyclic sediment transfer along and across convergent plate boundaries (Barbados, Lesser Antilles). Basin Research, 27, 696-713.

Marsaglia, K.M., Ingersoll, R.V., 1992. Compositional trends in arc-related, deep-marine sand and sandstone: a reassessment of magmatic-arc provenance. Geological Society of America Bulletin, 104, 1637-1649.

Morozova, G.S., 2005. A review of Holocene avulsions of the Tigris and Euphrates rivers and possible effects on the evolution of civilizations in lower Mesopotamia. Geoarchaeology 20, 401-423.

Nesbitt, H.W., Young, G.M., 1982. Early Proterozoic climates and plate motions inferred from major element chemistry of lutites. Nature, 299, 715-717.

Oberhänsli, R., Candan, O., Bousquet, R., Rimmele, G., Okay, A., Goff, J., 2010. Alpine high pressure evolution of the eastern Bitlis complex, SE Turkey. Geological Society London, Special Publications 340, 461-483.

Okay, A.I., 2008. Geology of Turkey: a synopsis. Anschnitt 21, 19-42.

Parker, A., 1970. An index of weathering for silicate rocks. Geological Magazine, 107, 501-504.

Partow, H., 2001. The Mesopotamian marshlands: demise of an ecosystem, UNIP/DEWA/TR,01-3, early warning and assessment technical report, United Nations Environmental Programme, Nairobi, Kenya, 58 pp.

Pearce, J.A., Bender, J.F., De Long, S.E., Kidd, W.S.F., Low, P.J., Güner, Y., Saroglu, F., Yilmaz, Y., Moorbath, S., Mitchell, J.G., 1990. Genesis of collision volcanism in Eastern Anatolia, Turkey. Journal of Volcanology and Geothermal Research 44, 189-229.

Phillip, G., 1968. Mineralogy of recent sediments of Tigris and Euphrates rivers and some of the older detrital deposits. Journal of Sedimentary Petrology 38, 35-44.

Rice, S.P., Robertson, A., Ustaömer, T., İnan, N., Tasli, K., 2009. Late Cretaceous-Early Eocene tectonic development of the Tethyan suture zone in the Erzincan area, Eastern Pontides, Turkey. Geological Magazine, 146, 567-590.

Ricou, L.E., 1971, Le croissant ophiolitique péri-arabe: une ceinture de nappes mises en place Crétacé supérieur: Revue de Géographie Physique et de Géologie Dynamique 13, 327-349.

Robertson, A.H.F., Parlak, O., Rízaoğlu, T., Ünlügenç, Ü, İnan, N., Tasli, K., Ustaömer, T., 2007 Tectonic evolution of the South Tethyan ocean: evidence from the Eastern Taurus Mountains (Elaziğ region, SE Turkey). Geological Society London, Special Publication 272, 231-270.

Robertson, A.H.F., Parlak, O., Ustaömer, T., 2013a. Late Palaeozoic–Early Cenozoic tectonic development of Southern Turkey and the easternmost Mediterranean region: evidence from the inter-relations of continental and oceanic units. Geological Society London, Special Publication 372, 9-48.

Robertson, A.H.F., Parlak, O., Metín, Y., Vergílí, Ö., Tasli, K., İnan, N., Soycan, H., 2013b. Late Palaeozoic–Cenozoic tectonic development of carbonate platform, margin and oceanic units in the Eastern Taurides, Turkey. Geological Society London, Special Publication 372, 167-218.

Salarijazi, M., Akhond-Ali, A.M., Abdi, A., Daneshkhah, A., 2012. Trend and change-point detection for the annual stream-flow series of the Karun River at the Ahvaz hydrometric station. African Journal of Agricultural Research 7, 4540-4552.

Sarifakioğlu, E., Özen, H., Winchester, J.A., 2009. Petrogenesis of the Refahiye Ophiolite and its tectonic significance for Neotethyan ophiolites along the İzmir-Ankara-Erzincan Suture Zone. Turkish Journal of Earth Sciences, 18, 187-207.

Şengör, A.M.C., Özeren, S., Genç, T., Zor, E., 2003. East Anatolian high plateau as a mantle-supported, north-south shortened domal structure. Geophysical Research Letters, 30 (24), 8045, doi:10.1029/2003GL017858, 2003.

Sepehr, M., Cosgrove, J.W., 2004. Structural framework of the Zagros Fold-Thrust Belt, Iran. Marine and Petroleum Geology 21, 829-843.

Shahzad, F., Gloaguen, R., 2011. TecDEM: a MATLAB based toolbox for tectonic geomorphology, part 1: drainage network pre-processing and stream profile analysis. Computer and Geosciences 37, 250-260.

Sláma, J., Košler, J., Condon, D.J., Crowley, J.L., Gerdes, A., Hanchar, J.M., Horstwood, M.S.A., Morris, G.A., Nasdala, L., Norberg, N., Schaltegger, U., Schoene, B., Tubrett, M.N., Whitehouse, M.J., 2008. Plešovice zircon - a new natural reference material for U-Pb and Hf isotopic microanalysis. Chemical Geology, 249, 1-35.

Stocklin, J., 1968. Structural history and tectonics of Iran: a review. American Association of Petroleum Geologists Bulletin 52, 1229-1258.

Szabo, F., Kheradpir, A., 1978. Permian and Triassic stratigraphy, Zagros Basin, South-West Iran. Journal of Petroleum Geology, 1, 2, 57-82.

Taylor and McLennan, 1995 Taylor, S. R., and McLennan, S. M. 1995. The geochemical evolution of the continental crust. Reviews of Geophysics, 33, 241-265.

Teller, J.T., Glennie, K.W., Lancaster, N., Singhvi, A.K., 2000. Calcareous dunes of the United Arab Emirates and Noah's flood: the postglacial reflooding of the Persian (Arabian) Gulf. Quaternary International 68-71, 297-308.

Thornburg, T.M., Kulm, L.D., 1987. Sedimentation in the Chile Trench: petrofacies and provenance. Journal of Sedimentary Petrology 57, 55-74.

Uchupi, E., Swift, S.A., Ross, D.A., 1999. Late Quaternary stratigraphy, paleoclimate and neotectonism of the Persian (Arabian) Gulf region. Marine Geology 160, 1-23.

Ustaömer, P.A., Ustaömer, T., Gerdes, A., Robertson, A.H.F., Collins, A.S., 2012. Evidence of Precambrian sedimentation/magmatism and Cambrian metamorphism in the Bitlis Massif, SE Turkey utilising whole-rock geochemistry and U–Pb LA-ICP-MS zircon dating. Gondwana Research 21, 1001-1018.

Vermeesch, P., 2012. On the visualisation of detrital age distributions. Chemical Geology, 312-313, 190-194.

Vermeesch, P., Resentini, A., Garzanti, E., 2016. An R package for statistical provenance analysis. Sedimentary Geology, 336, 14-25.

Vezzoli, G., Garzanti, E., Vincent, S.J., Andó, S., Carter, A., Resentini, A., 2014. Tracking sediment provenance and erosional evolution of the western Greater Caucasus. Earth Surface Processes and Landforms 39, 1101-1114.

Whitechurch, H., Omrani, J., Agard, P., Humbert, F., Montigny, R., Jolivet, L., 2013. Evidence for Paleocene–Eocene evolution of the foot of the Eurasian margin (Kermanshah ophiolite, SW Iran) from back-arc to arc: Implications for regional geodynamics and obduction. Lithos, 182-183, 11-32.

Wilkinson, T.J., Rayne, L., Jotheri, J., 2015. Hydraulic landscapes in Mesopotamia: the role of human niche construction. Water History 7, 397-418

Wobus, C.W., Hodges, K.V., Whipple, K.X., 2003. Has focused denudation sustained active thrusting at the Himalayan topographic front ? Geology 31, 861-864

Yerino, L.N., Maynard, J.B., 1984. Petrography of modern marine sands from the Peru-Chile Trench and adjacent areas. Sedimentology 31, 83-89.

Yiğitbaş, E., Yilmaz, Y., 1996. New evidence and solution to the Maden complex controversy of the Southeast Anatolian orogenic belt (Turkey). Geologische Rundschau 85, 250-263.

Yilmaz, Y., 1993. New evidence and model on the evolution of the southeast Anatolian orogen. Geological Society of America Bulletin 105, 251-271.

Yılmaz, Y., Güner, Y., Şaroğlu, F., 1998. Geology of the Quaternary volcanic centres of the East Anatolia. Journal of Volcanology and Geothermal Research 85, 173-210.

Yilmaz, Y., Yiğitbaş, E., Genç, Ş., 1993. Ophiolitic and metamorphic assemblages of southeast Anatolia and their significance in the geological evolution of the orogenic belt. Tectonics 12, 1280-1297.

Zuffa, G.G., 1985. Optical analyses of arenites: influence of methodology on compositional results. In: Zuffa, G.G. (Ed.), Provenance of arenites. Reidel, Dordrecht, NATO ASI Series 148, pp. 165-189.

The Euphrates-Tigris-Karun river system: provenance, recycling and dispersal of quartz-poor foreland-basin sediments in arid climate

ABSTRACT

We present a detailed sediment-provenance study on the modern Euphrates-Tigris-Karun fluvial system and Mesopotamian foreland basin, one of the cradles of humanity. Our rich petrographic and heavy-mineral dataset, integrated by sand geochemistry and U-Pb age spectra of detrital zircons, highlights the several peculiarities of this large source-to-sink sediment-routing system and widens the spectrum of compositions generally assumed as paradigmatic for orogenic settings. Comparison of classical static versus upgraded dynamic petrologic models enhance the power of provenance analysis, and allow us to derive a more refined conceptual model of reference and to verify the limitations of the approach.

Sand derived from the Anatolia-Zagros orogen contains abundant lithic grains eroded from carbonates, cherts, mudrocks, arc volcanics, obducted ophiolites and ophiolitic mélanges representing the exposed shallow structural level of the orogen, with relative scarcity of quartz, K-feldspar and mica. This quartz-poor petrographic signature, characterizing the undissected composite tectonic domain of the entire Anatolia-Iranian plateau, is markedly distinct from that of sand shed by more elevated and faster-eroding collision orogens such as the Himalaya. Arid climate in the region allows preservation of chemically unstable grains including carbonate rock fragments and locally even gypsum, and reduces transport capacity of fluvial systems, which dump most of their load in Mesopotamian marshlands upstream of the Arabian/Persian Gulf allochemical carbonate factory. Quartz-poor sediment from the Anatolia-Zagros orogen mixes with quartz-rich recycled sands from Arabia along the western side of the foreland basin, and is traced all along the Gulf shores as far as the Rub' al-Khali sand sea up to 4000 km from Euphrates headwaters.

Table 1

	N	Q	F	Lvm	Lc	Ls	Lsm	Lm	Lu		P/F	MI	tHMC	ZTR	Ttn	Ap	Ep	Grt	And	Amp	Cpx	En	Hy	Ol	Sp	&tHM		HCl
MOUNTAIN STREAMS																												
Erzincan suture	2	**4**	**22**	**26**	**13**	**1**	**5**	**1**	**27**	100.0	**96**	**69**	**8.6**	**0**	**0**	**1**	**11**	**2**	**0**	**24**	**57**	**1**	**1**	**1**	**2**	**0**	100.0	**47**
(upper Karasu)		*1*	*11*	*1*	*3*	*2*	*1*	*1*	*10*		*4*	*44*	*0.9*	*0*	*0*	*1*	*9*	*2*	*0*	*5*	*19*	*1*	*1*	*2*	*0*	*0*		*6*
Tauride platform	6	**14**	**19**	**22**	**31**	**1**	**3**	**4**	**5**	100.0	**94**	**108**	**4.0**	**1**	**0**	**2**	**21**	**3**	**0**	**26**	**40**	**2**	**1**	**1**	**2**	**0**	100.0	**30**
(+ophiolite & lava)		*13*	*13*	*16*	*24*	*1*	*3*	*3*	*7*		*4*	*51*	*1.6*	*1*	*0*	*4*	*13*	*6*	*0*	*12*	*16*	*2*	*0*	*1*	*0*	*0*		*15*
Sanandaj-Sirjan Zone	4	**19**	**13**	**8**	**21**	**0**	**37**	**2**	**0**	100.0	**86**	**73**	**6.2**	**0**	**0**	**1**	**40**	**3**	**0**	**37**	**18**	**0**	**0**	**0**	**0**	**0**	100.0	**43**
(in Iran)		*8*	*9*	*7*	*7*	*0*	*9*	*2*	*0*		*8*	*42*	*4.4*	*0*	*0*	*1*	*33*	*3*	*0*	*26*	*17*	*0*	*0*	*0*	*0*	*0*		*30*
Bitlis suture	1	25	34	26	1	1	3	9	2	100.0	94	183	13.9	1	0	1	19	2	0	44	32	0	0	0	0	0	100.0	3
Zagros suture	12	**6**	**11**	**17**	**13**	**6**	**15**	**26**	**6**	100.0	**97**	**212**	**16.2**	**0**	**0**	**0**	**26**	**0**	**0**	**58**	**14**	**0**	**1**	**1**	**0**	**0**	100.0	**10**
(in Iraq and Iran)		*4*	*7*	*10*	*8*	*7*	*9*	*25*	*5*		*5*	*116*	*14.1*	*0*	*0*	*0*	*8*	*1*	*0*	*21*	*19*	*0*	*2*	*1*	*1*	*0*		*10*
Meso-Cenozoic strata	2	**2**	**3**	**6**	**27**	**18**	**42**	**1**	**1**	100.0	94	**34**	**0.6**	**0**	**0**	**3**	**53**	**2**	**0**	**37**	**3**	**0**	**1**	**0**	**1**	**0**	100.0	n.d.
(suture zone)		*3*	*4*	*9*	*19*	*10*	*11*	*1*	*1*			*24*	*0.5*	*0*	*0*	*3*	*17*	*2*	*0*	*17*	*1*	*0*	*1*	*0*	*1*	*0*		
Mesozoic strata	3	**9**	**3**	**6**	**52**	**7**	**21**	**2**	**0**	100.0	**93**	**72**	**0.3**	**13**	**0**	**3**	**33**	**5**	**0**	**13**	**23**	**0**	**0**	**0**	**9**	**0**	100.0	**21**
(simply folded belt)		*3*	*1*	*5*	*19*	*6*	*13*	*2*	*0*		*12*	*27*	*0.2*	*9*	*0*	*1*	*19*	*5*	*0*	*12*	*17*	*0*	*0*	*0*	*5*	*1*		*4*
Cenozoic strata	2	**9**	**3**	**12**	**21**	**30**	**22**	**1**	**1**	100.0	**58**	**69**	**0.9**	**1**	**1**	**2**	**83**	**3**	**1**	**3**	**2**	**0**	**0**	**0**	**2**	**0**	100.0	n.d.
(simply folded belt)		*6*	*1*	*2*	*2*	*8*	*2*	*1*	*1*		*12*	*50*	*0.7*	*1*	*0*	*1*	*9*	*3*	*1*	*1*	*3*	*0*	*1*	*0*	*0*	*0*		
EUPHRATES SYSTEM																												
Karasu	1	3	34	51	11	0	0	0	0	100.0	99	3	5.5	0	0	0	1	0	0	14	63	1	19	2	0	0	100.0	83
Murat	1	31	27	27	5	1	2	5	1	100.0	93	152	7.5	0	1	1	26	6	0	33	28	0	1	0	0	2	100.0	0
Euphrates	3	**33**	**23**	**17**	**15**	**3**	**3**	**3**	**4**	100.0	**78**	**99**	**6.8**	**0**	**0**	**2**	**33**	**3**	**0**	**27**	**29**	**0**	**4**	**1**	**1**	**0**	100.0	**29**
(west-central Iraq)		*2*	*7*	*3*	*2*	*2*	*1*	*1*	*3*		*3*	*15*	*2.5*	*0*	*1*	*1*	*5*	*2*	*0*	*3*	*2*	*0*	*1*	*1*	*1*	*0*		*5*
Euphrates *(S Iraq)*	1	49	17	6	23	4	1	1	1	100.0	77	141	2.3	4	0	4	35	15	1	23	11	0	0	0	6	0	100.0	21
TIGRIS SYSTEM																												
Upper Tigris	1	26	26	19	13	1	8	4	5	100.0	84	144	7.9	2	0	0	43	3	1	11	25	2	0	10	0	0	100.0	15
Batman	1	54	21	4	4	1	3	11	3	100.0	79	304	4.5	1	1	1	29	22	1	40	3	0	0	0	0	0	100.0	13
Khabour	1	20	10	15	38	3	13	1	1	100.0	69	48	0.7	1	5	3	37	4	0	17	13	0	0	0	14	4	100.0	39
Tigris	3	**32**	**11**	**10**	**25**	**8**	**8**	**4**	**1**	100.0	**73**	**143**	**3.0**	**2**	**1**	**3**	**28**	**11**	**1**	**29**	**17**	**0**	**0**	**0**	**2**	**5**	100.0	**17**
(north Iraq)		*11*	*2*	*6*	*5*	*4*	*4*	*3*	*0*	36.6	*10*	*47*	*0.6*	*1*	*1*	*1*	*10*	*11*	*2*	*10*	*8*	*0*	*0*	*0*	*0*	*5*		*4*
Greater Zab	1	9	6	21	30	2	25	2	6	100.0	89	39	4.6	0	2	2	17	0	0	22	54	0	0	0	1	1	100.0	20
Lesser Zab	3	**17**	**8**	**7**	**26**	**3**	**20**	**13**	**6**	100.0	**80**	**196**	**5.3**	**2**	**1**	**2**	**16**	**3**	**10**	**50**	**14**	**0**	**0**	**0**	**2**	**0**	100.0	**29**
(middle course)		*8*	*5*	*4*	*8*	*5*	*7*	*8*	*7*		*11*	*33*	*2.9*	*1*	*1*	*3*	*4*	*2*	*15*	*14*	*9*	*1*	*1*	*0*	*1*	*0*		*10*
Lesser Zab	3	**21**	**9**	**13**	**24**	**9**	**18**	**3**	**3**	100.0	**72**	**88**	**1.9**	**2**	**1**	**1**	**42**	**7**	**3**	**27**	**11**	**0**	**0**	**0**	**2**	**3**	100.0	**35**
(lower course)		*7*	*0*	*5*	*2*	*2*	*3*	*1*	*1*		*16*	*11*	*0.9*	*2*	*1*	*0*	*8*	*1*	*2*	*5*	*6*	*0*	*0*	*0*	*2*	*1*		*10*
Tigris + dune	2	**53**	**15**	**6**	**15**	**5**	**4**	**2**	**0**	100.0	**61**	**92**	**1.4**	**5**	**2**	**0**	**53**	**22**	**0**	**11**	**2**	**0**	**0**	**0**	**2**	**3**	100.0	17
(central Iraq)		*3*	*2*	*0*	*4*	*5*	*3*	*1*	*0*		*2*	*50*	*0.8*	*3*	*0*	*0*	*13*	*5*	*0*	*1*	*2*	*0*	*0*	*0*	*2*	*3*		*n.d.*
Diyala	2	**11**	**9**	**13**	**25**	**30**	**10**	**1**	**1**	100.0	**85**	**56**	**1.4**	**0**	**0**	**0**	**35**	**3**	**0**	**13**	**48**	**0**	**1**	**0**	**0**	**0**	100.0	**52**
		3	*5*	*1*	*1*	*10*	*3*	*1*	*1*		*15*	*3*	*0.2*	*0*	*0*	*0*	*16*	*0*	*0*	*9*	*24*	*0*	*1*	*0*	*1*	*0*		*10*
Tigris	3	**31**	**11**	**6**	**32**	**4**	**9**	**4**	**4**	100.0	**80**	**157**	**3.5**	**2**	**1**	**1**	**36**	**15**	**0**	**26**	**14**	**0**	**0**	**0**	**3**	**1**	100.0	**22**
(lower course)		*6*	*2*	*2*	*2*	*3*	*2*	*1*	*3*		*5*	*15*	*1.1*	*1*	*1*	*1*	*10*	*8*	*0*	*14*	*7*	*0*	*0*	*0*	*2*	*2*		*12*
MESOPOTAMIA																												
East of Euphrates	13	**27**	**23**	**12**	**25**	**1**	**3**	**4**	**5**	100.0	**85**	**148**	**7.3**	**1**	**1**	**1**	**25**	**4**	**0**	**38**	**27**	**0**	**1**	**0**	**2**	**1**	100.0	**18**
		4	*3*	*4*	*3*	*1*	*1*	*2*	*2*		*4*	*22*	*3.0*	*1*	*0*	*1*	*5*	*2*	*0*	*7*	*8*	*0*	*1*	*0*	*1*	*1*		*6*
West of Euphrates	3	**69**	**12**	**3**	**8**	**0**	**1**	**3**	**4**	100.0	**70**	**165**	**2.9**	**4**	**1**	**1**	**31**	**4**	**0**	**25**	**30**	**1**	**1**	**0**	**1**	**1**	100.0	**28**
		22	*4*	*4*	*6*	*0*	*1*	*3*	*6*		*12*	*35*	*3.5*	*3*	*1*	*1*	*8*	*3*	*0*	*4*	*13*	*1*	*0*	*0*	*0*	*1*		*7*
IRAN, GULF & ARABIA																												
Karkeh	2	**12**	**9**	**5**	**45**	**21**	**8**	**1**	**0**	100.0	**76**	**86**	**0.8**	**3**	**0**	**2**	**39**	**7**	**3**	**17**	**19**	**0**	**0**	**0**	**9**	**1**	100.0	**42**
(lower course)		*2*	*1*	*1*	*14*	*10*	*3*	*1*	*0*		*4*	*42*	*0.4*	*2*	*0*	*0*	*13*	*2*	*1*	*7*	*10*	*0*	*0*	*0*	*1*	*0*		*2*
Karun	4	**10**	**3**	**1**	**72**	**7**	**6**	**0**	**0**	100.0	**73**	**56**	**0.5**	**8**	**0**	**3**	**35**	**9**	**1**	**17**	**13**	**0**	**0**	**0**	**13**	**0**	100.0	**30**
(lower course)		*2*	*1*	*1*	*2*	*2*	*2*	*0*	*0*		*7*	*15*	*0.2*	*1*	*0*	*1*	*9*	*3*	*1*	*5*	*5*	*0*	*0*	*0*	*7*	*1*		*11*
Shatt al-Arab	4	**9**	**3**	**3**	**60**	**16**	**8**	**1**	**0**	100.0	**63**	**34**	**0.2**	**3**	**0**	**1**	**46**	**7**	**2**	**11**	**21**	**0**	**0**	**0**	**6**	**2**	100.0	**38**
		0	*2*	*2*	*12*	*12*	*3*	*0*	*0*		*18*	*4*	*0.2*	*2*	*1*	*1*	*7*	*4*	*1*	*3*	*3*	*1*	*0*	*0*	*2*	*1*		*8*
Wadi al-Batin	1	94	2	1	4	0	0	0	0	100.0	43	n.d.	0.4	41	1	0	9	0	0	33	12	0	0	0	0	2	100.0	24
Kuwait beach	1	89	9	1	1	0	0	0	0	100.0	52	n.d.	0.03	6	1	1	45	7	0	15	22	2	1	0	1	2	100.0	30

Table 2

Click here to download Table: Table 2 Mesopotamia.pdf

Table 2

River	SiO_2	Al_2O_3	Fe_2O_3	MgO	CaO	Na_2O	K_2O	TiO_2	P_2O_5	MnO	LOI	Rb	Sr	Ba	Sc	Y	La	Sm	Eu	Gd	Yb	Th	U	Zr	V	Nb	Cr	Co	Ni
	wt%	wt%	wt%	wt%	wt%	wt%	wt%	wt%	wt%	wt%	wt%	ppm	ppm	ppm	ppm	ppm	ppm	ppm	ppm	ppm	ppm	ppm	ppm	ppm	ppm	ppm	ppm	ppm	ppm
TIGRIS																													
Tigris@Diyarbakir	56.5	10.4	6.5	4.2	9.0	2.4	1.2	0.7	0.26	0.09	8.5	26	215	185	15	18	18	3	0.8	3.3	1.7	6	3	104	169	9	889	28	159
Batman	72.9	9.5	3.6	2.3	3.5	2.7	1.4	0.5	0.10	0.06	3.3	32	136	292	8	16	21	4	0.7	3.2	1.7	6	2	113	63	7	404	11	75
Tigris@Sohaila	63.2	8.1	3.8	2.8	9.7	2.0	1.2	0.6	0.07	0.08	8.2	28	210	209	8	16	17	3	0.7	2.8	1.6	5	2	103	70	8	787	10	70
Greater Zab	45.9	9.2	6.1	6.3	14.3	1.5	1.3	0.7	0.12	0.10	14.1	33	268	206	16	16	17	3	0.9	3.2	1.6	3	2	89	138	9	684	21	180
Lesser Zab	58.2	8.3	3.7	2.9	12.4	1.3	1.2	0.4	0.07	0.08	11.3	35	180	185	9	13	14	2	0.7	2.4	1.4	4	1	74	85	5	445	10	78
Aq Su	78.7	4.5	2.0	0.9	6.1	0.7	0.8	0.2	0.05	0.03	6.1	22	135	250	4	9	8	2	0.4	1.6	0.8	2	1	49	46	4	75	5	26
Diyala	77.4	4.5	2.1	0.9	6.8	0.8	0.8	0.2	0.07	0.03	6.4	19	150	221	4	9	8	1	0.4	1.5	0.8	3	1	47	42	3	41	6	28
Tigris@Baghdad	53.2	8.2	4.5	2.8	14.1	1.6	1.2	0.8	0.08	0.11	13.0	32	247	239	10	19	19	3	0.7	3.1	1.9	4	1	184	106	11	2189	17	78
Tigris@Numaniyah	55.7	8.3	3.5	3.2	13.6	1.9	1.2	0.5	0.07	0.08	11.7	30	224	202	9	14	13	3	0.6	2.8	1.5	4	1	91	79	6	677	12	92
EUPHRATES																													
Karasu	56.6	15.2	4.7	2.8	8.5	3.4	1.5	0.8	0.15	0.07	6.1	41	364	287	12	15	17	3	0.9	2.7	1.4	5	2	122	92	8	192	15	64
Murat	59.3	13.5	6.5	2.9	6.1	3.3	1.6	1.0	0.18	0.11	5.2	43	245	266	17	23	19	4	1.0	4.1	2.3	6	1	150	146	10	281	17	66
Euphrates@AlQaim	53.0	11.2	5.8	4.5	12.3	2.4	0.9	0.8	0.09	0.11	8.6	23	296	196	18	17	15	3	0.9	3.1	1.8	3	1	89	164	7	992	19	107
Euphrates@Ramadi	61.3	9.9	3.7	3.6	9.6	2.3	1.1	0.5	0.07	0.07	7.7	27	250	237	10	13	11	2	0.7	2.2	1.3	3	1	73	92	5	376	13	107
Euphrates@Nasiriyah	73.6	5.2	1.7	1.4	7.8	1.1	1.3	0.2	0.06	0.04	7.4	30	253	274	4	8	8	1	0.4	1.3	0.8	2	1	73	34	4	260	5	42
KARUN																													
Karkheh	51.2	4.5	2.2	1.8	19.9	0.8	0.9	0.3	0.07	0.05	18.1	24	289	178	5	10	13	2	0.5	1.9	1.0	3	1	75	54	4	753	7	41
Dez	65.1	1.8	1.4	1.0	15.6	0.2	0.4	0.1	0.06	0.02	14.4	10	283	103	2	6	8	1	0.3	1.1	0.6	1	1	29	39	2	41	3	<20
Upper Karun	25.4	1.6	1.0	2.2	36.6	0.3	0.4	0.1	0.04	0.03	32.2	9	366	76	2	6	7	1	0.3	1.0	0.5	1	2	39	31	1	144	3	<20
Karun	31.1	3.0	2.1	3.2	30.4	0.5	0.5	0.3	0.07	0.05	28.4	14	369	94	4	9	13	2	0.5	1.9	0.9	2	2	95	54	4	1081	7	35
Shatt al-Arab	31.9	2.5	1.6	2.5	31.7	0.4	0.5	0.2	0.06	0.05	28.5	13	386	82	3	8	9	1	0.4	1.4	0.7	2	2	54	41	3	322	6	31
WADI AL-BATIN	91.6	1.5	0.5	0.9	1.8	0.1	0.5	0.1	0.03	<0.01	3.0	10	54	109	1	4	9	1	0.3	1.0	0.6	2	1	240	13	2	<14	1	<20

Figure 1
Click here to download high resolution image

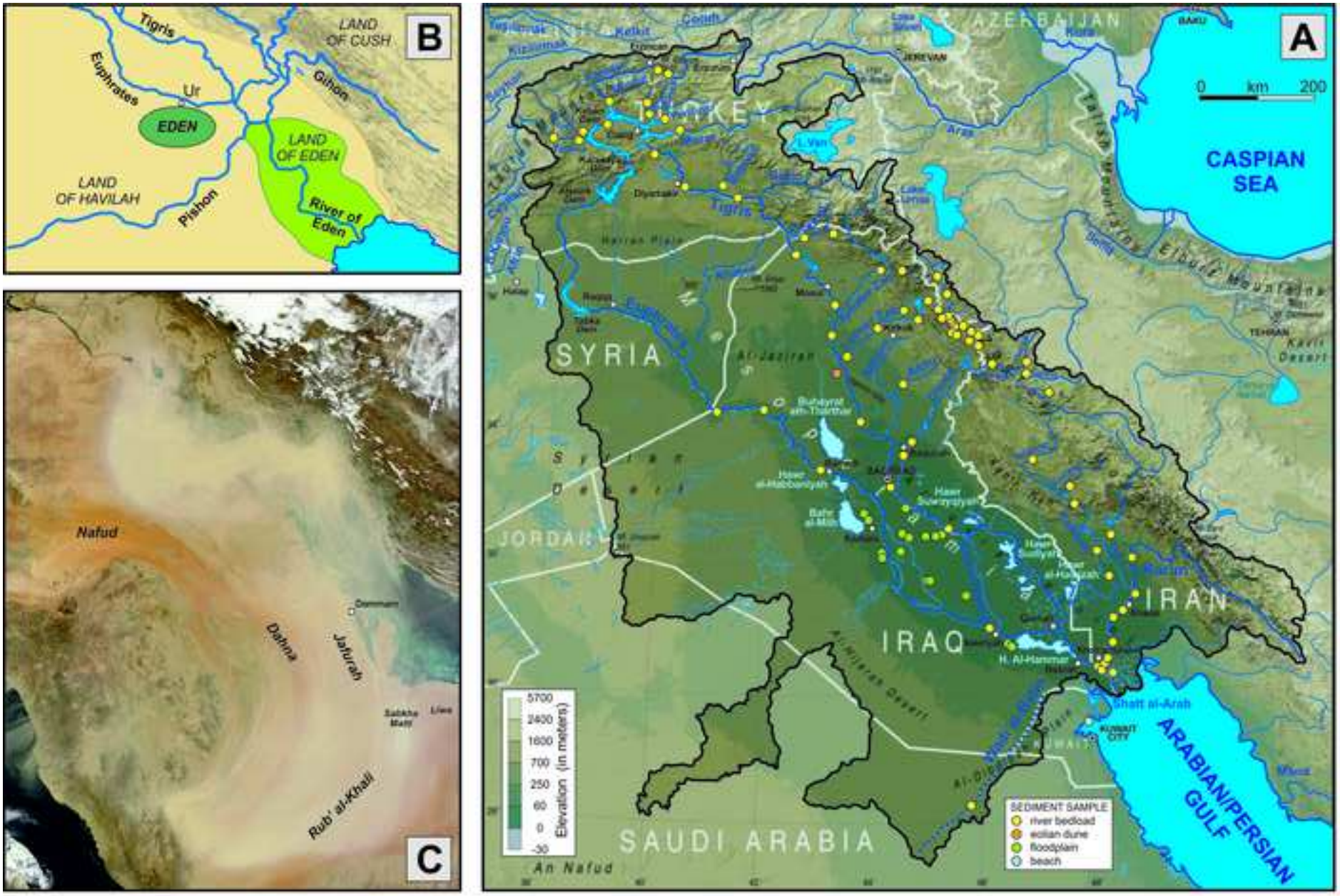

Figure 1 Mesopotamia

Figure 2
Click here to download high resolution image

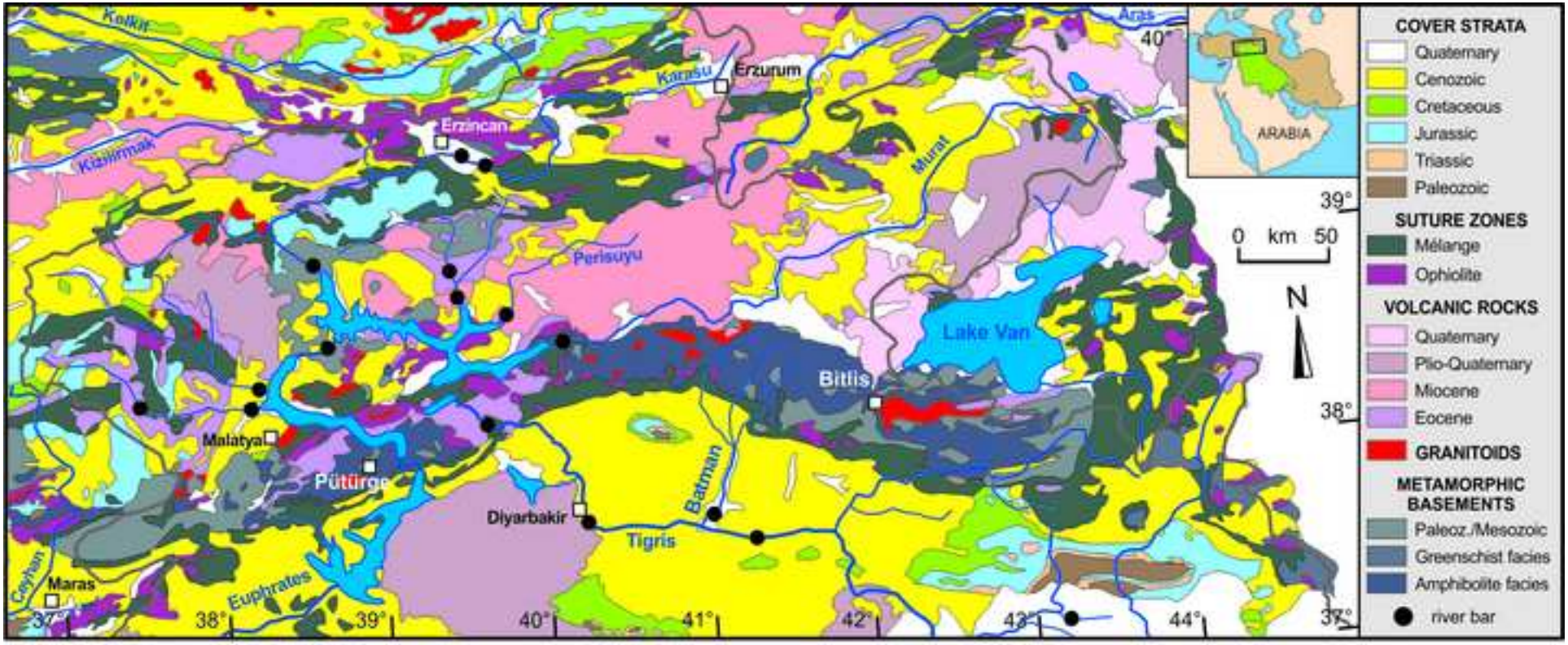

Figure 2 Mesopotamia

Figure 3

Click here to download high resolution image

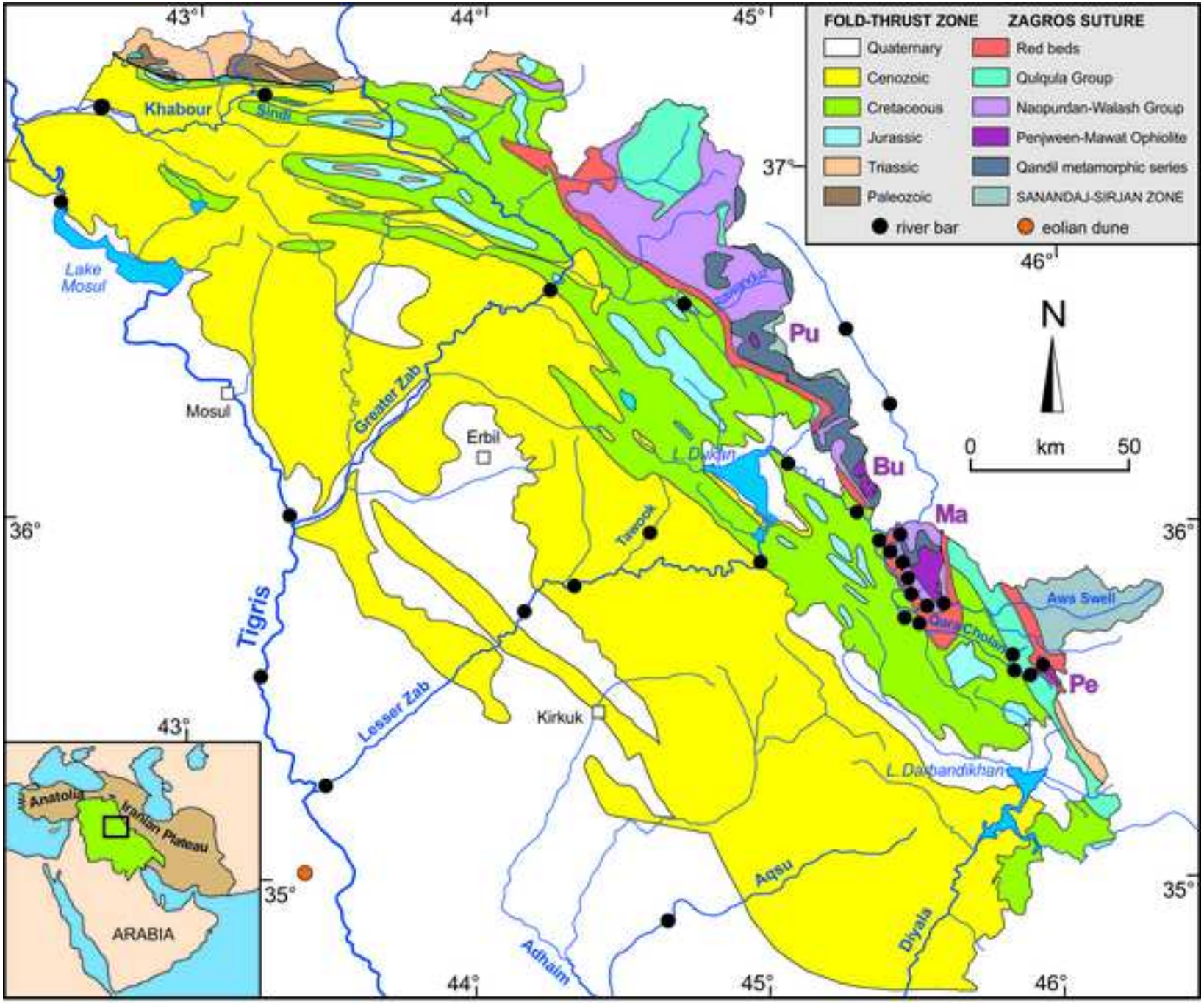

Figure 3 Mesopotamia

Figure 4
Click here to download high resolution image

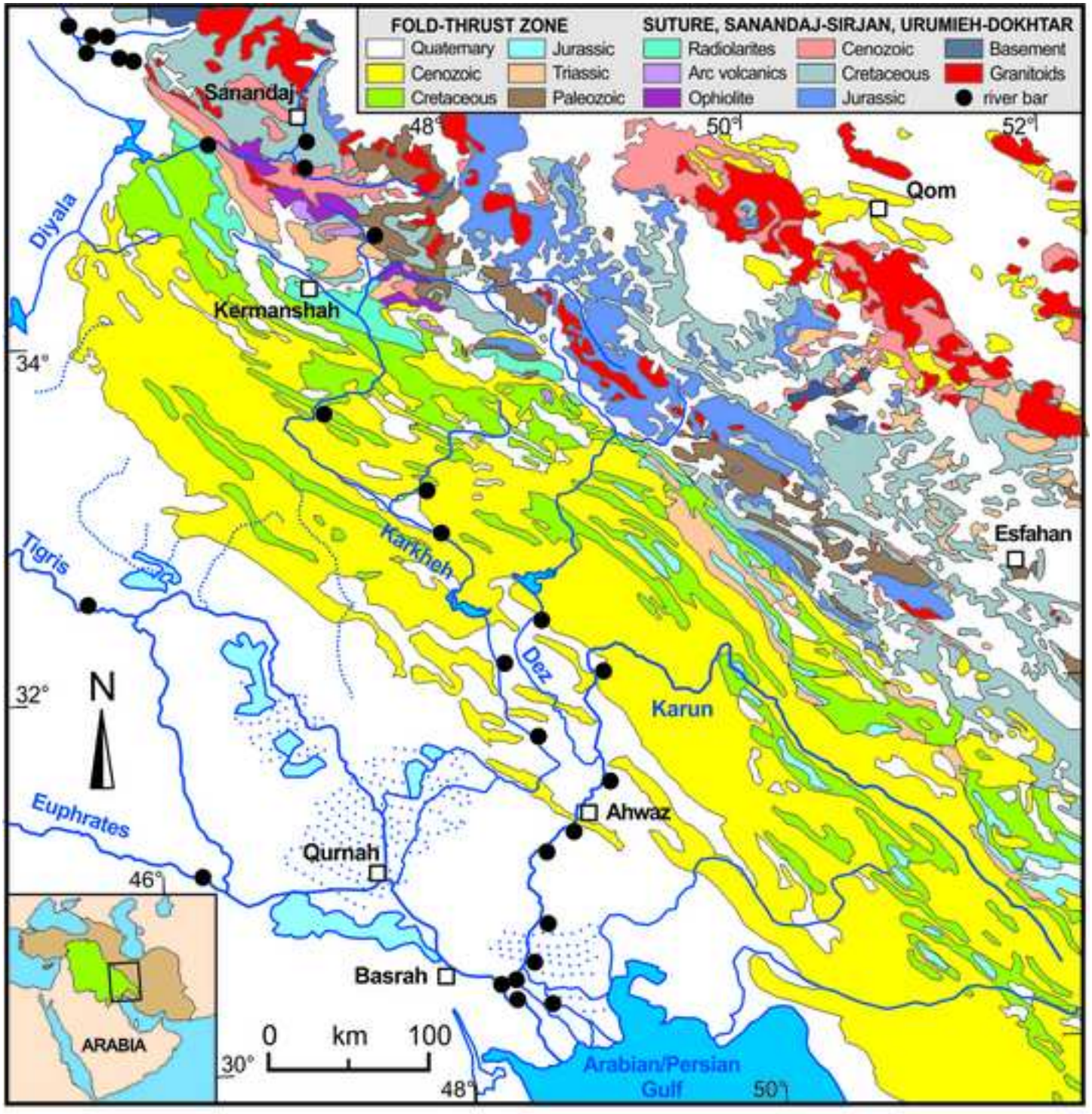

Figure 4 Mesopotamia

Figure 5

Click here to download high resolution image

Figure 5 Mesopotamia

Figure 6

Click here to download high resolution image

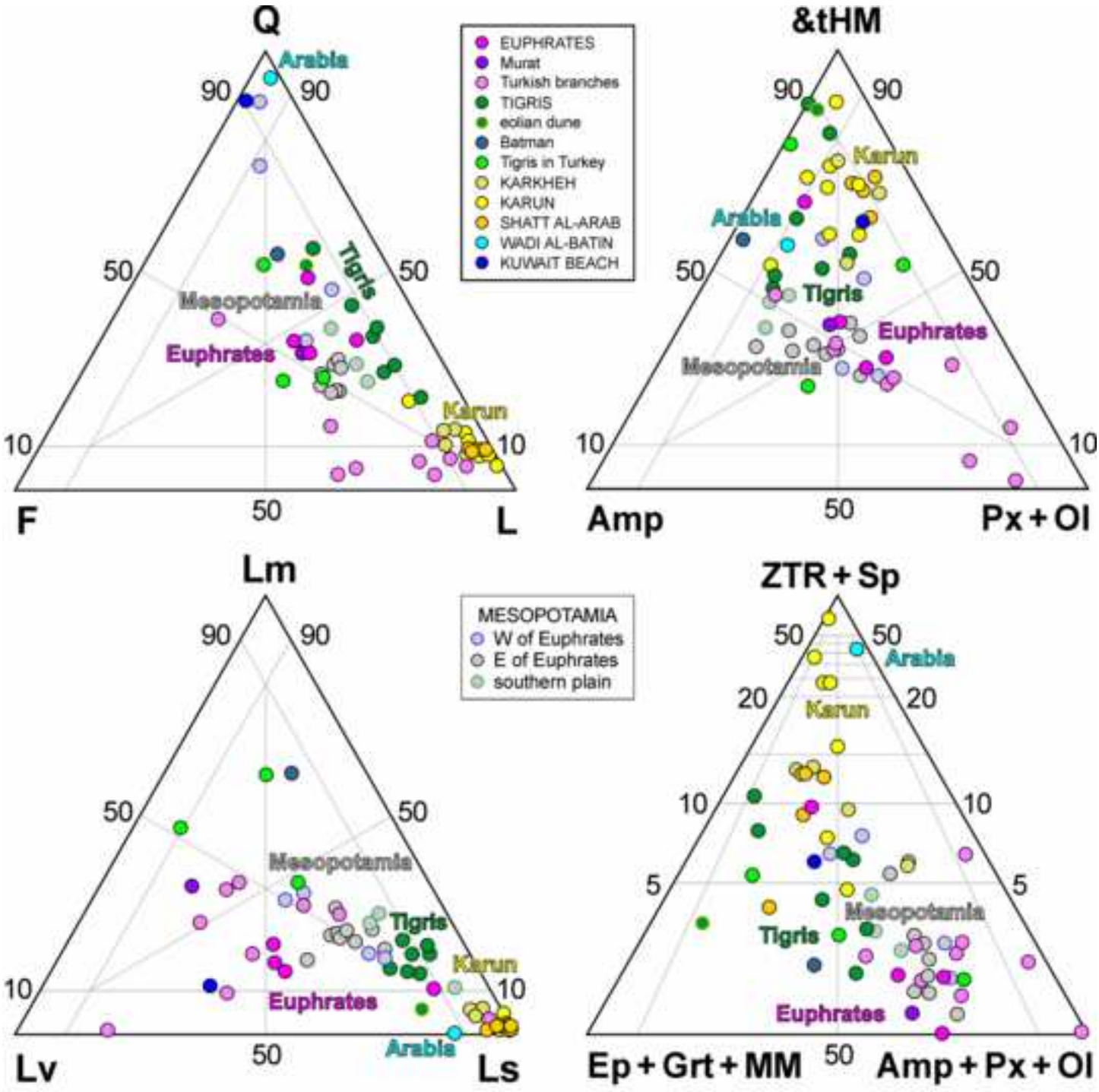

Figure 6 Mesopotamia

Figure 7

Click here to download high resolution image

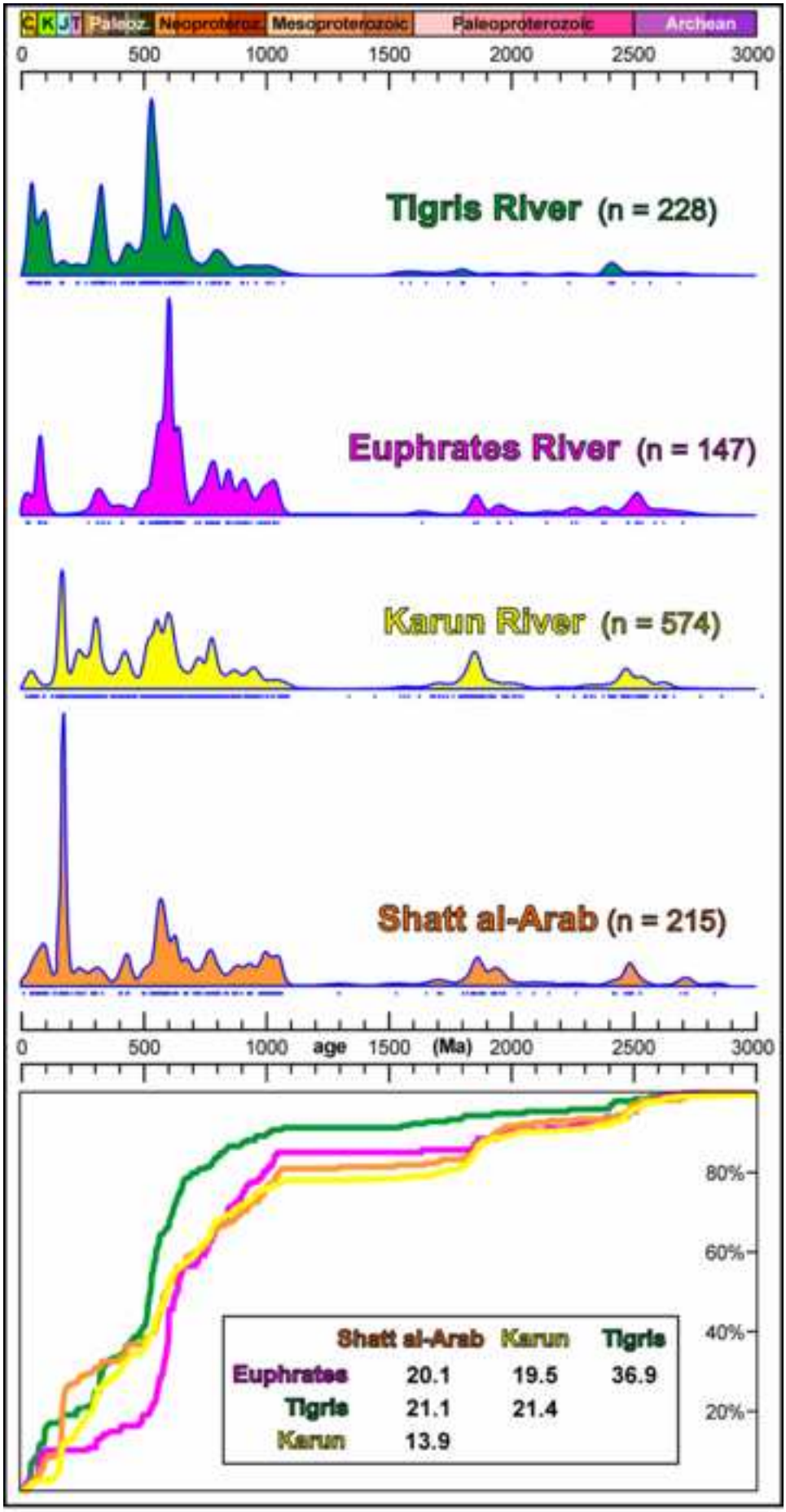

Figure 7 Mesopotamia

Figure 8
Click here to download high resolution image

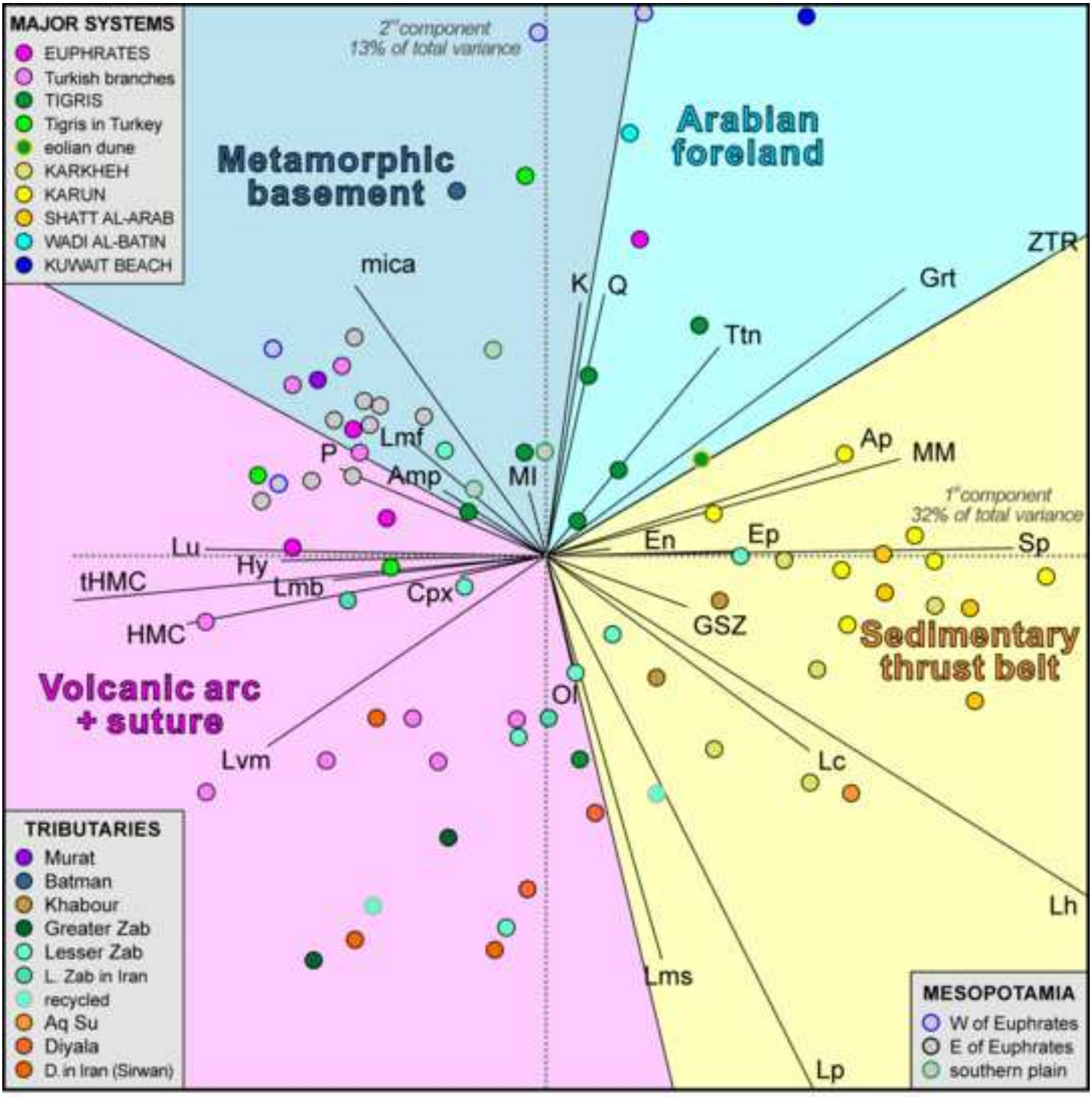

Figure 8 Mesopotamia

Figure 9
Click here to download high resolution image

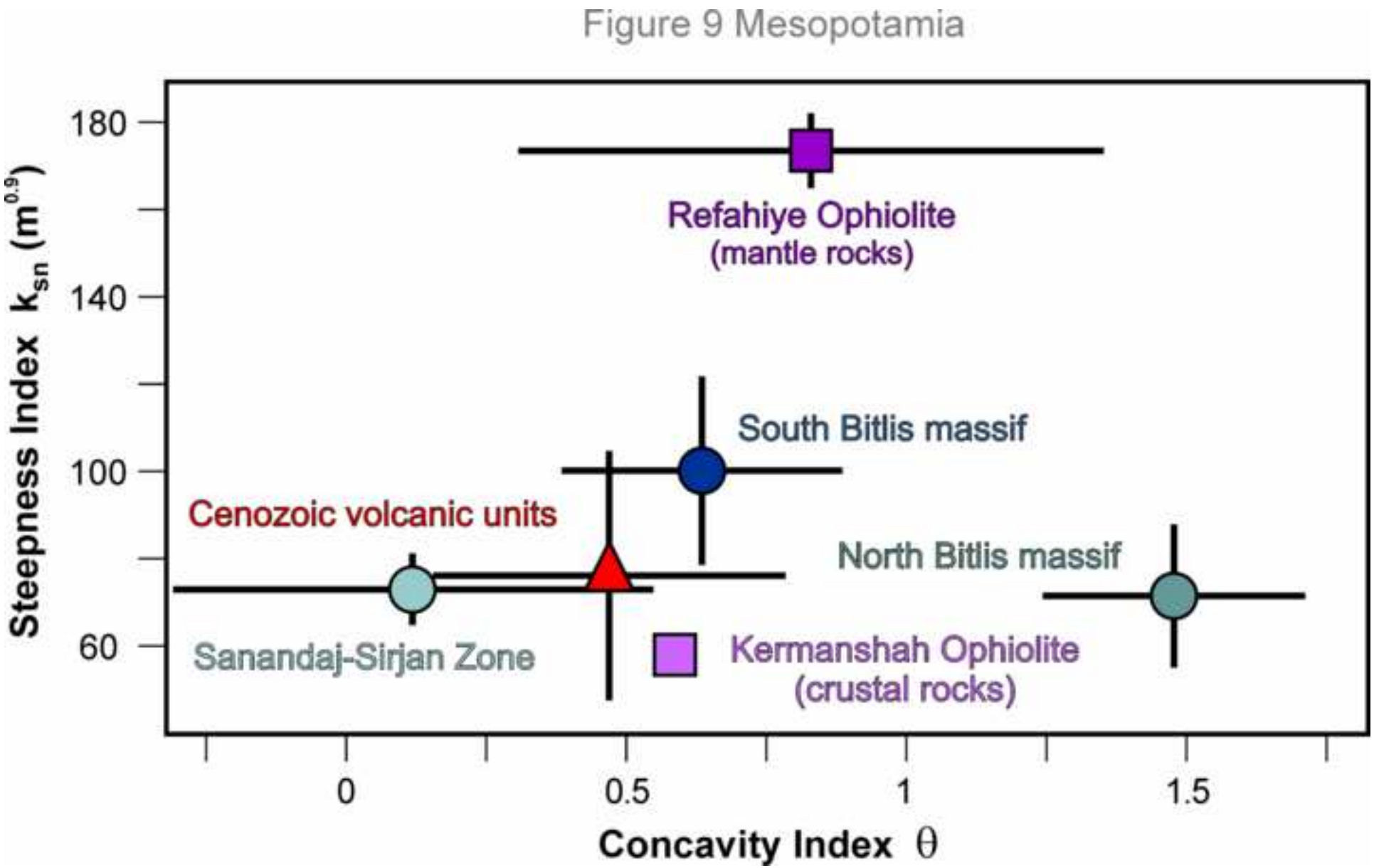

Figure 10
Click here to download high resolution image

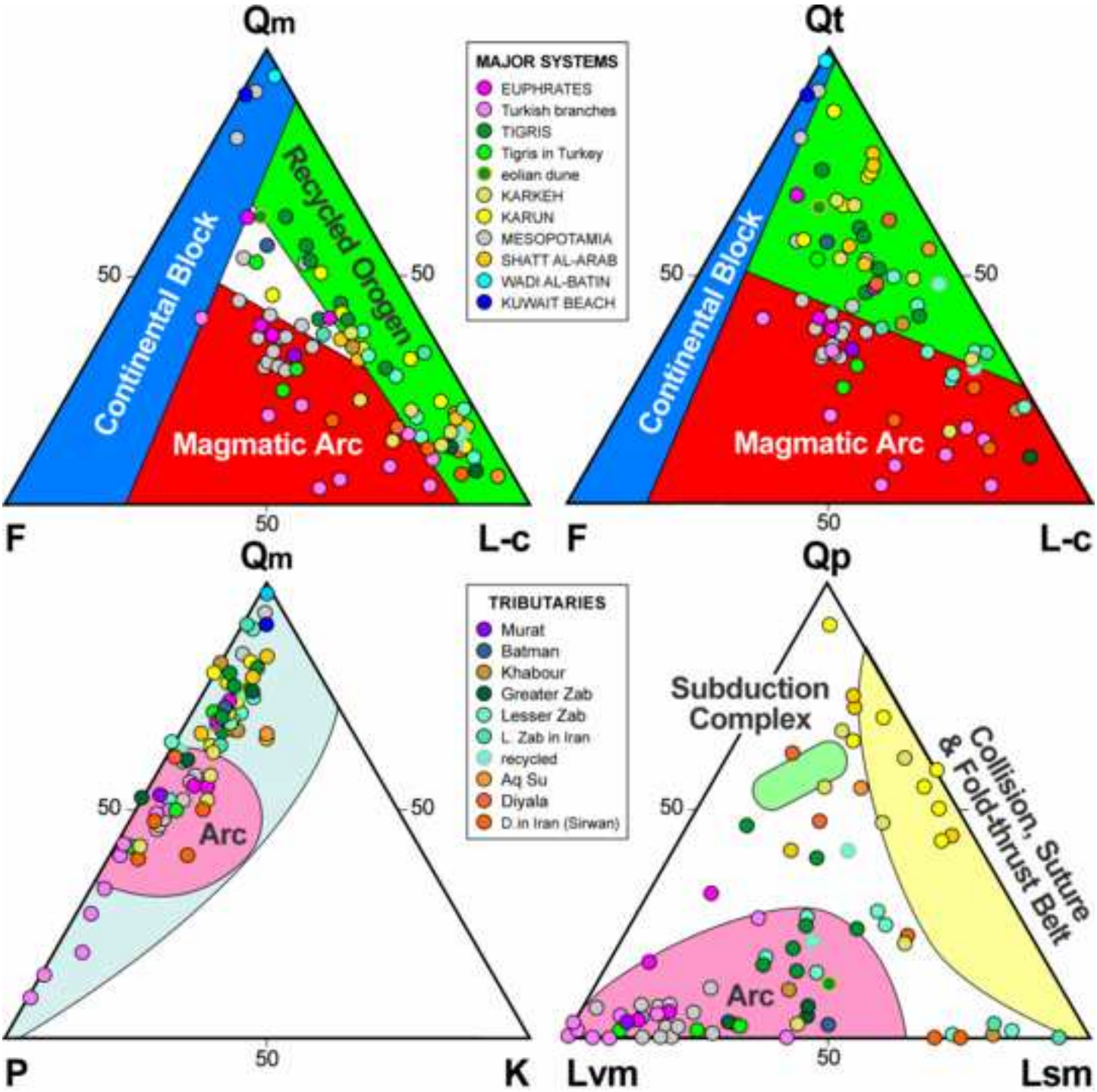

Figure 10 Mesopotamia

Figure 11

Click here to download high resolution image

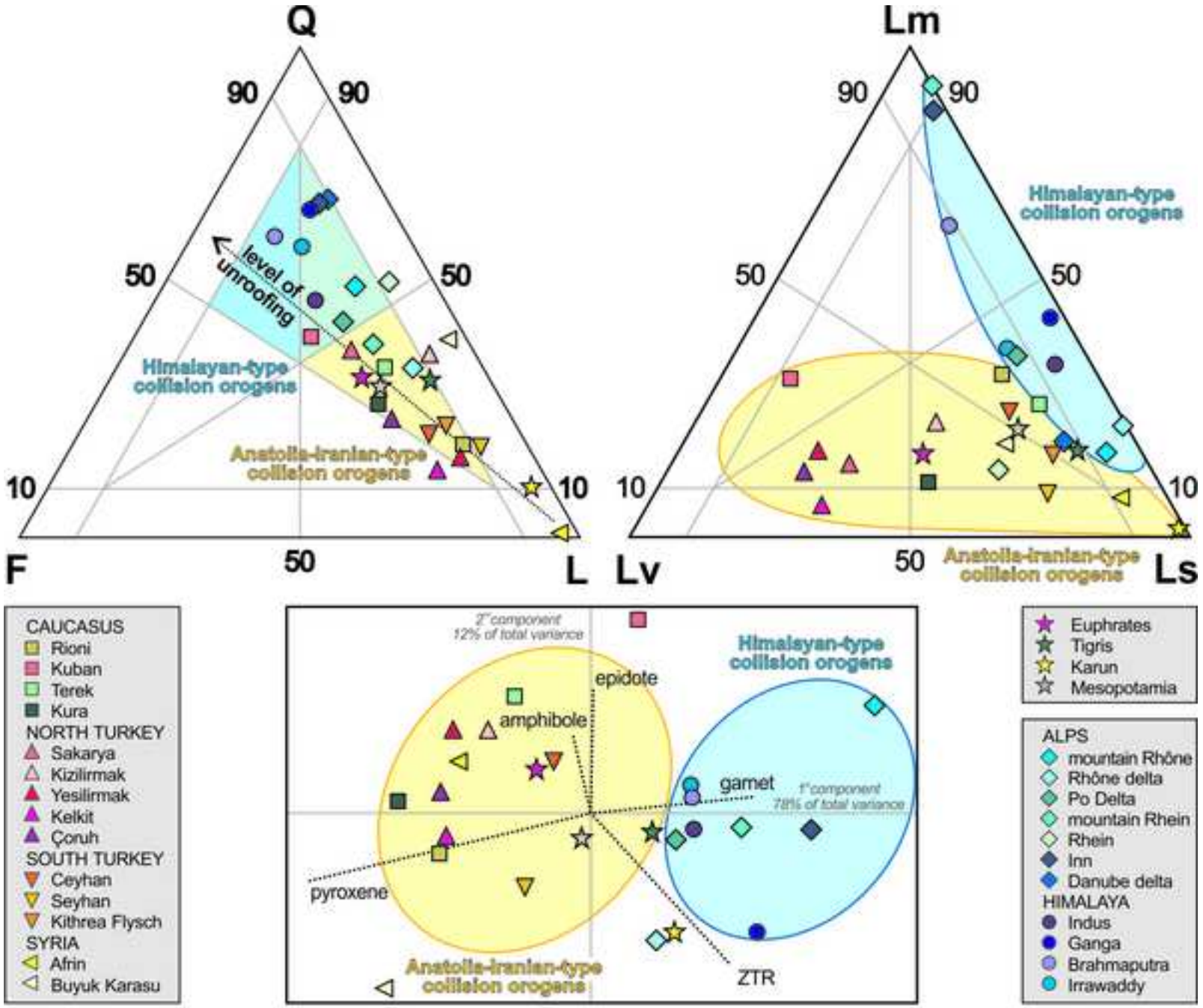

Figure 11 Mesopotamia